Journal Name

ARTICLE TYPE

Supporting Information for "Future costs of power-to-liquid sustainable aviation fuels produced from hybrid solar PV-wind plants in Europe"[†]

Kyle Seymour,*[a] Maximilian Held,[a] Boris Stolz,[b] Gil Georges,[a] and Konstantinos Boulouchos[a]

This Supporting Information document contains the following additional information:

1. Code access via GitHub

2. Jet fuel properties

3. Plant operation optimsation (constraints and optimisation target)

4. Component cost projections (CAPEX)

5. Electricity generation resources (solar PV, onshore and offshore wind)

6. Wind turbine selection

7. Hourly operation example

8. Installed component capacities (result of optimiser)

9. Storage discharge times

10. Curtailment of electricity (result of optimiser)

11. Domestic PtL-SAF cost production curves (for all individual countries in Europe)

12. Green premium and GHG abatement costs of PtL-SAF production

13. Plant cost breakdown

[a] ETH Zurich; Department of Mechanical and Process Engineering; Institute of Energy Technology; Leonhardstrasse 21, 8092 Zurich, Switzerland
[b] Federal Department of the Environment, Transport, Energy and Communications; Federal Office of Civil Aviation; Mühlestrasse 2, 3063 Ittigen, Switzerland
† Electronic Supplementary Information (ESI) available: [details of any supplementary information available should be included here]. See DOI: 00.0000/00000000.
* Corresponding author: Kyle Seymour, Email: kwdseymour@gmail.com

1   Code access via GitHub

The code developed for the analysis in this paper is made openly available via GitHub at `https://github.com/kwdseymour/EuroSAFs` to facilitate a more complete understanding of the methods used and to allow researchers to expand upon this work. Additionally, the GitHub repository will house additional analyses and tools as they become available (such as a land cover type visualizer).

2   Jet fuel properties

Table 1 documents the density, lower heating value and tank-to-wake emission factor of jet fuel.

Table 1 Properties of kerosene-type jet fuel used in this study.

	Value	Reference
Density in l/kg	1.25	1
LHV in MJ/kg	44.1	2
Emission factor in kg CO_2/kg fuel	3.16	3

3 Plant operation optimisation

The plant operation optimiser is mathematically defined by the equalities and constraints provided in this section. All variables defining the optimisation problem are depicted in the flow chart in Figure 1. Hourly variables are denoted with the subscript, i. The accompanying file "plant_assumptions.xlsx" contains definitions and units for all variables.
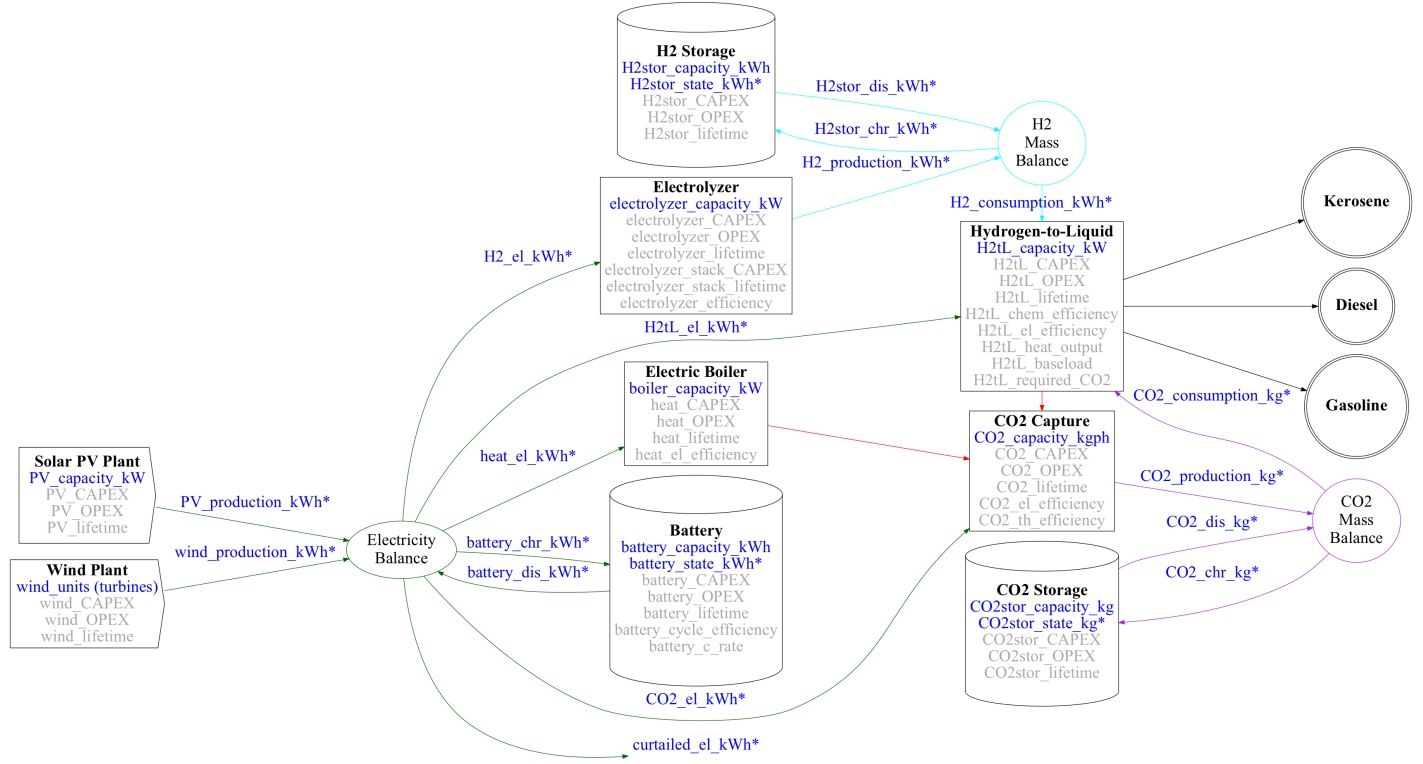

Figure 1 Plant flowchart illustrating how optimisation variables relate to the energy and mass balances. Green arrows represent flow of electricity, red represents heat, light blue represents hydrogen, purple represents carbon dioxide, and black represents fuel. Variables in blue are optimiser decision variables and asterisks indicate those that are hourly. Grey variables are exogenous specifications.

$$H2\_production\_kWh_i = H2\_el\_kWh_i \cdot electrolyser\_efficiency \tag{1}$$

$$H2\_consumption\_kWh_i = H2\_production\_kWh_i + H2stor\_dis\_kWh_i - H2stor\_chr_kWh_i \tag{2}$$

$$fuel\_production\_kWh_i = H2\_consumption\_kWh_i \cdot H2tL\_chem\_efficiency \cdot kerosene\_energy\_fraction \tag{3}$$

$$CO2\_production\_kg_i = \frac{CO2\_el\_kWh_i}{CO2\_el\_efficiency} \tag{4}$$

$$CO2\_consumption\_kg_i = CO2\_production\_kg_i + CO2stor\_dis\_kg_i - CO2stor\_chr\_kg_i \tag{5}$$

3.1 Constraints

$$curtailed\_el\_kWh_i \leq wind\_production\_kWh_i + PV\_production\_kWh_i \tag{6}$$

$$wind\_production\_kWh_i + PV\_production\_kWh_i + battery\_dis\_kWh_i =$$
$$curtailed\_el\_kWh_i + battery\_chr\_kWh_i + H2\_el\_kWh_i + CO2\_el\_kWh_i + H2tL\_el\_kWh_i + heat\_el\_kWh_i \tag{7}$$

$$heat\_el\_kWh_i \cdot heat\_el\_efficiency + fuel\_production\_kWh_i \cdot H2tL\_heat\_output \geq \frac{CO2\_production\_kg_i}{CO2\_th\_efficiency} \tag{8}$$

Equations 9 and 10 apply to battery, hydrogen and carbon dioxide storage types, while equation 11 applies only to hydrogen and carbon dioxide storage types.

$$storage\_state_i \leq storage\_capacity \tag{9}$$

$$storage\_state_1 = storage\_state_{8760} \tag{10}$$

$$stor\_state_{i+1} = stor\_state_i + stor\_chr_i - stor\_dis_i \tag{11}$$

$$battery\_state\_kWh_{i+1} = battery\_state\_kWh_i + battery\_chr\_kWh_i \cdot \sqrt{battery\_cycle\_efficiency} - \frac{battery\_dis\_kWh_i}{\sqrt{battery\_cycle\_efficiency}} \tag{12}$$

$$battery\_chr\_kWh_i \leq battery\_capacity\_kWh \cdot battery\_c\_rate \tag{13}$$

$$battery\_dis\_kWh_i \leq battery\_capacity\_kWh \cdot battery\_c\_rate \tag{14}$$

$$H2\_el\_kWh_i \leq electrolyser\_capacity\_kW \tag{15}$$

$$H2\_el\_kWh_i \geq electrolyser\_baseload \cdot electrolyser\_capacity\_kW \tag{16}$$

$$CO2\_production\_kg_i \leq CO2\_capacity\_kgph \tag{17}$$

$$heat\_el\_kWh_i \leq boiler\_capacity\_kW \tag{18}$$

$$fuel\_production\_kWh_i \leq H2tL\_capacity\_kW \tag{19}$$

$$fuel\_production\_kWh_i \geq H2tL\_capacity\_kW \cdot H2tL\_baseload \tag{20}$$

$$CO2\_consumption\_kg_i = H2\_consumption\_kWh_i \cdot H2tL\_required\_CO2 \tag{21}$$

$$H2tL\_el\_kWh_i = fuel\_production\_kWh_i \cdot H2tL\_el\_demand \tag{22}$$

$$\sum_{i=1}^{8760} fuel\_production\_kWh_i \geq required\_fuel\_kWh \tag{23}$$

3.2 Optimisation target

The optimisation target is the minimisation of the NPV of total lifetime plant costs, as given in equations 24 and 25, where Θ represents component capacities.

$$Cost_{plant}(\Theta) = \sum_j \Theta_j \cdot NPV_j \tag{24}$$

$$min\, Cost_{plant}(\Theta) \tag{25}$$

4 Component cost projections

Component capital expenditures (CAPEX) are based on a literature review.[4–19] CAPEX values used in this study are based on the average cost of all literature values in 2020, C_0. Per component, the shape parameter, k, of the empirically defined CAPEX degression curve, $C(t)$, is defined such that the cost in 2050 matches again the average cost of all literature values in 2050:

$$C(t) = \frac{1}{2}\left(C_0 \, (1+t)^{-10k} + C_0 \, exp(-kt) \right) \tag{26}$$

with $0 < t < 30$, corresponding to the years 2020-2050. Figure 2 shows the literature data and the estimated values used in this study.

DAC cost projections vary considerably (see literature review in Figs. 3 and 4), in particular depending on the geographical location of the carbon capture plant[20]. Due to the high DAC costs (compared to point source capture of CO_2 from biomass or industrial plants) and the high uncertainty of future DAC costs (and the corresponding high investment risk), many PtL-SAF plants currently favour point sources of CO_2 (e.g., from cement of biomass plants). However, in the long run, PtL-SAF needs to be powered by DAC to guarantee a short-term closed carbon loop[21].
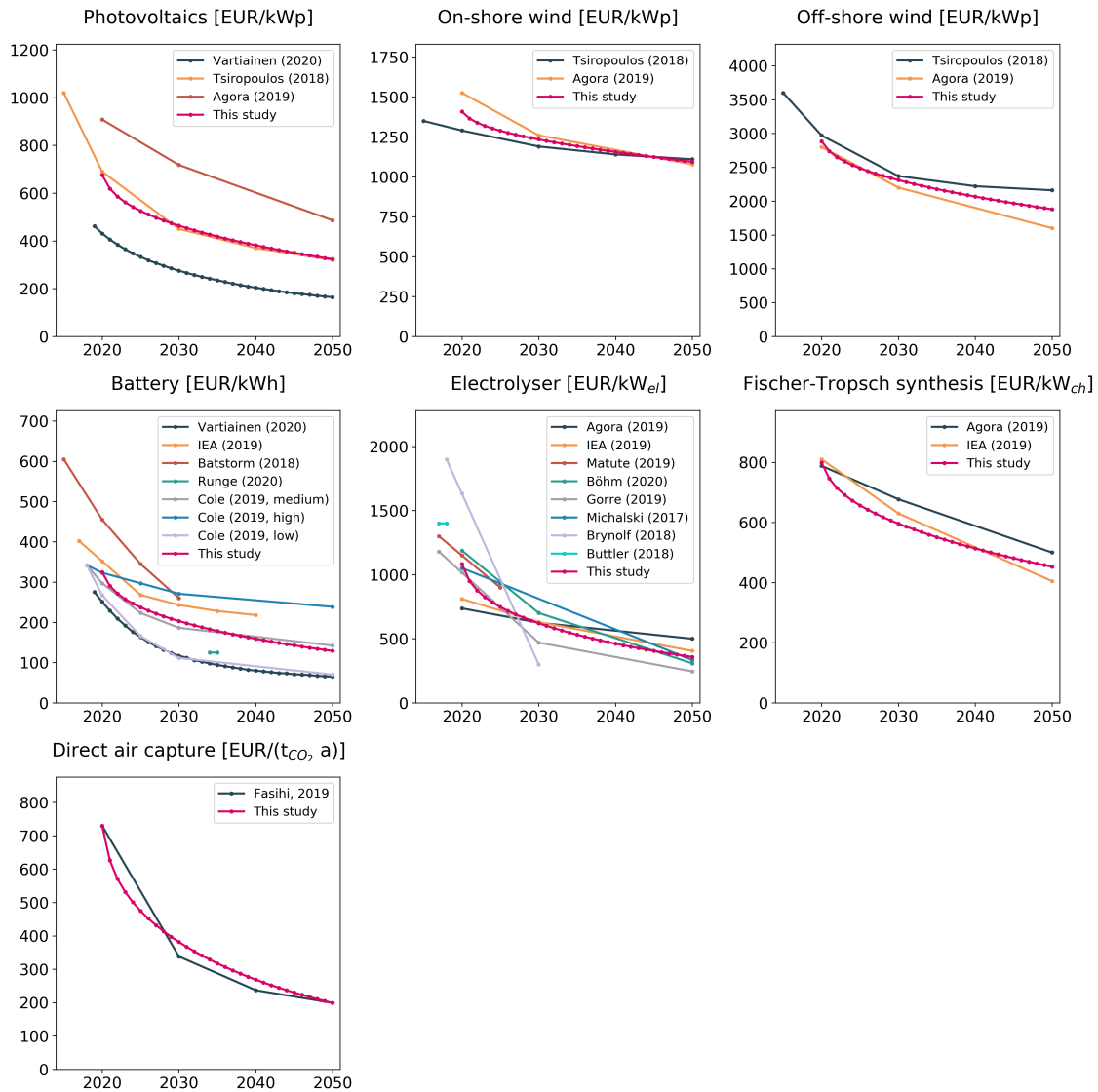
Figure 2 Literature review of CAPEX for the individual components of a jet fuel production plant. [4–19] For the cost projections used in this study, Eq. 26 has been fitted to the literature values. Literature values for 2020 have been interpolated if original sources did not provide data points for this year.
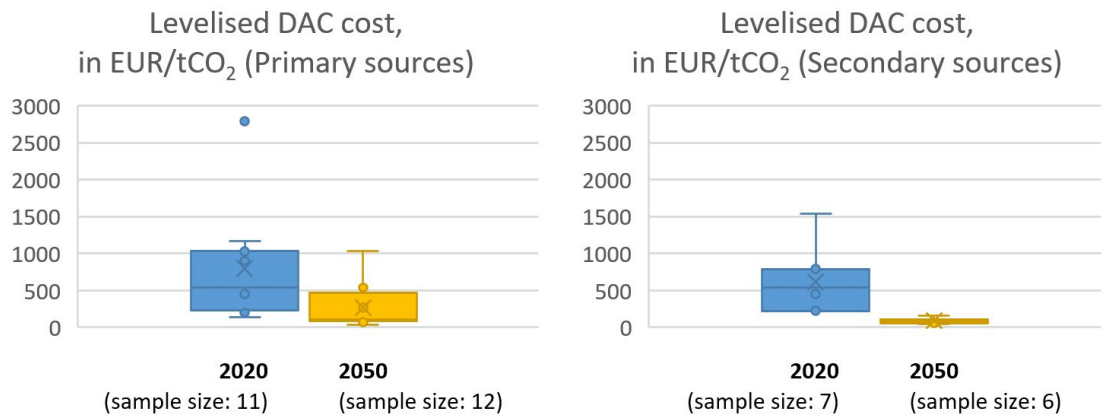
Figure 3 Literature review of levelised costs of direct air capture. Data from primary sources[18,22–25] resulting in the following median (20th, 80th percentile) values: 540 (230, 1030) EUR/tCO_2 in 2020 and 110 (80, 490) EUR/tCO_2 in 2050. Data from secondary sources[20,26–28] resulting in the following median (20th, 80th percentile) values: 540 (270, 740) EUR/tCO_2 in 2020 and 90 (60, 90) EUR/tCO_2 in 2050. Cost data includes a variety of different DAC types, e.g., liquid as well as solid sorbent DAC. Original figures in USD have been converted to EUR with an assumed exchange rate of 0.9 EUR/USD. 'First-of-a-kind' plants are assumed to be proxies for 2020, 'n-th-of-a-kind' plants are assumed to be proxies for 2050 cost data.
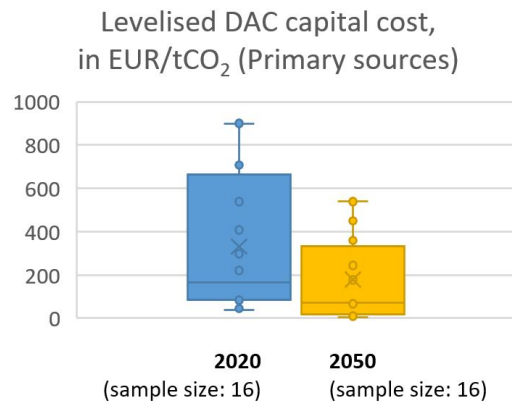
Figure 4 Literature review of levelised capital costs (CAPEX) of direct air capture. Data from refs.[23,24] resulting in the following median (20th, 80th percentile) values: 170 (80, 710) EUR/tCO_2 in 2020 and 70 (20, 360) EUR/tCO_2 in 2050. Cost data includes a variety of different DAC types, e.g., liquid as well as solid sorbent DAC. Original figures in USD have been converted to EUR with an assumed exchange rate of 0.9 EUR/USD. 'First-of-a-kind' plants are assumed to be proxies for 2020, 'n-th-of-a-kind' plants are assumed to be proxies for 2050 cost data.

5 Electricity generation resources

Figures 5-6 show the potential of solar PV and wind power across Europe. Offshore points are mapped to onshore locations where the rest of the fuel production plant would be located. The visual banding artifacts seen in Scandinavia are due to the use of different data sources by PVGIS around upper latitudes. PVGIS-SARAH is used for most of Europe and PVGIS-ERA5 is used for European latitudes above 60 N.
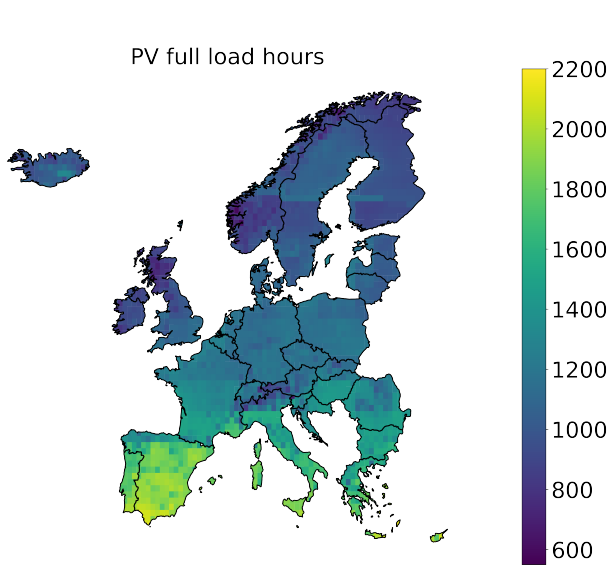

Figure 5 PV potential of fixed-tilt systems derived using PVGIS.
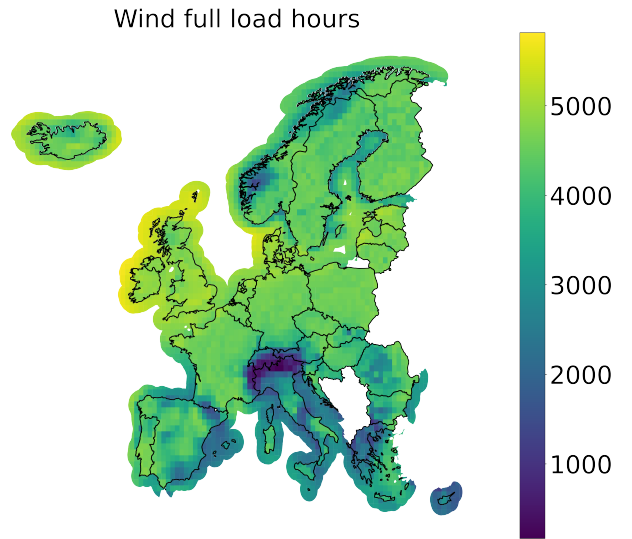
Figure 6 Wind potential derived from wind turbine power simulations.

6 Wind turbine selection and power calculation

Average wind speed was converted to power production using windpowerlib, an open-source Python library for simulating wind power production based on a database of wind turbine specifications.[29] For each of the turbine models in the database, the wind speed at each available hub height was calculated using the MERRA-2 50 meters wind speed and the Hellman exponential law:

$$v_{hub} = v_{ref} \cdot \left(\frac{h_{hub}}{h_{ref}} \right)^{\alpha} \tag{27}$$

where the wind speed, v_{hub}, at some hub height, h_{hub}, can be derived from a reference wind speed, v_{ref}, at some reference height, h_{ref}, using the Hellman exponent, α. The Hellman exponent for each node was derived using the MERRA-2 wind speeds at 10 and 50 meters and the same Equation 27. The theoretical full-load hours of all possible hub heights of each turbine model were calculated using the computed hourly average wind speed at hub height and the configuration with the highest full-load hours at each node was selected. Figure 7 shows the resulting optimised turbine model selection. The corresponding hourly power production per installed turbine was then determined for each location.
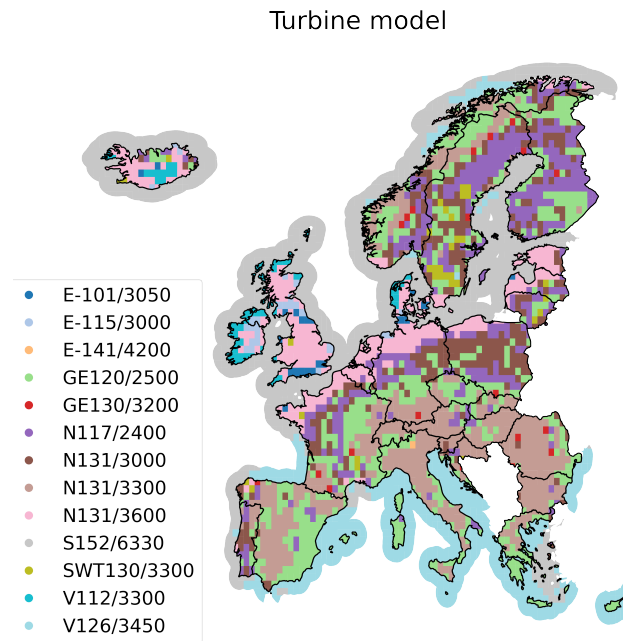
Figure 7 Optimal turbine model at each node based on full-load hours maximization.

7 Hourly operation example

Figure 8 shows the optimized hourly operation of an onshore plant in Poland during April of 2016. The battery capacity of this optimized plant (730 kWh) is in the 9th percentile of all evaluated locations and the LCOF is in the 12th percentile of all locations. This month had particularly low wind and PV resources, which reveals how the storage components are dispatched to ensure continuous production.
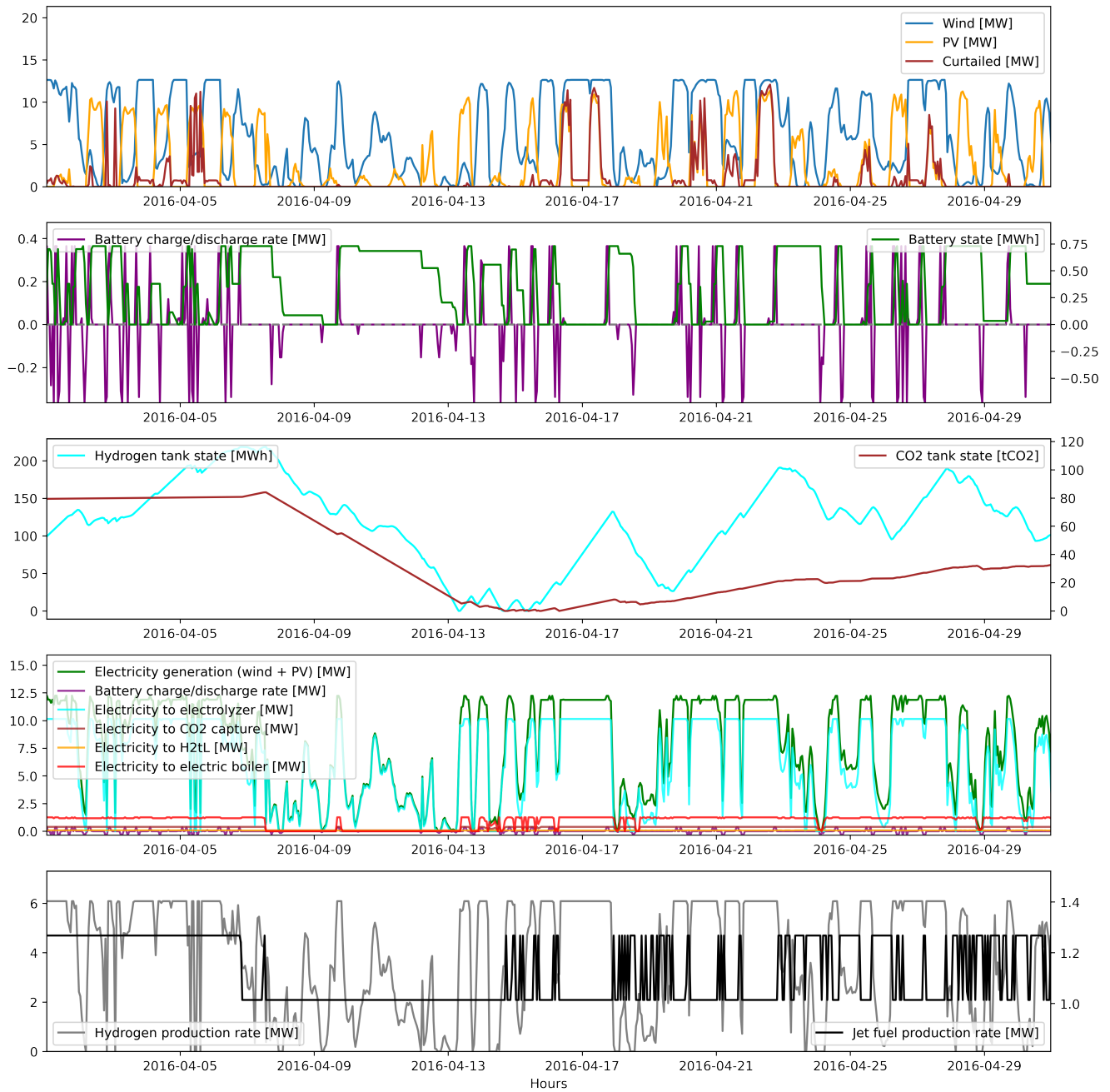
Figure 8 Optimized hourly plant operation of a plant in Poland during April of 2016. The plots represent, from top to bottom: electricity generation, battery operation, H_2 and CO_2 tank states, electricity consumption by various components, H_2 and fuel production rates.

8 Installed component capacities

The optimiser presented in this paper optimises the size, i.e. installed capacities, of all plant components and their operation. The resulting component capacities for the 2020 optimization are shown in Figure 9.
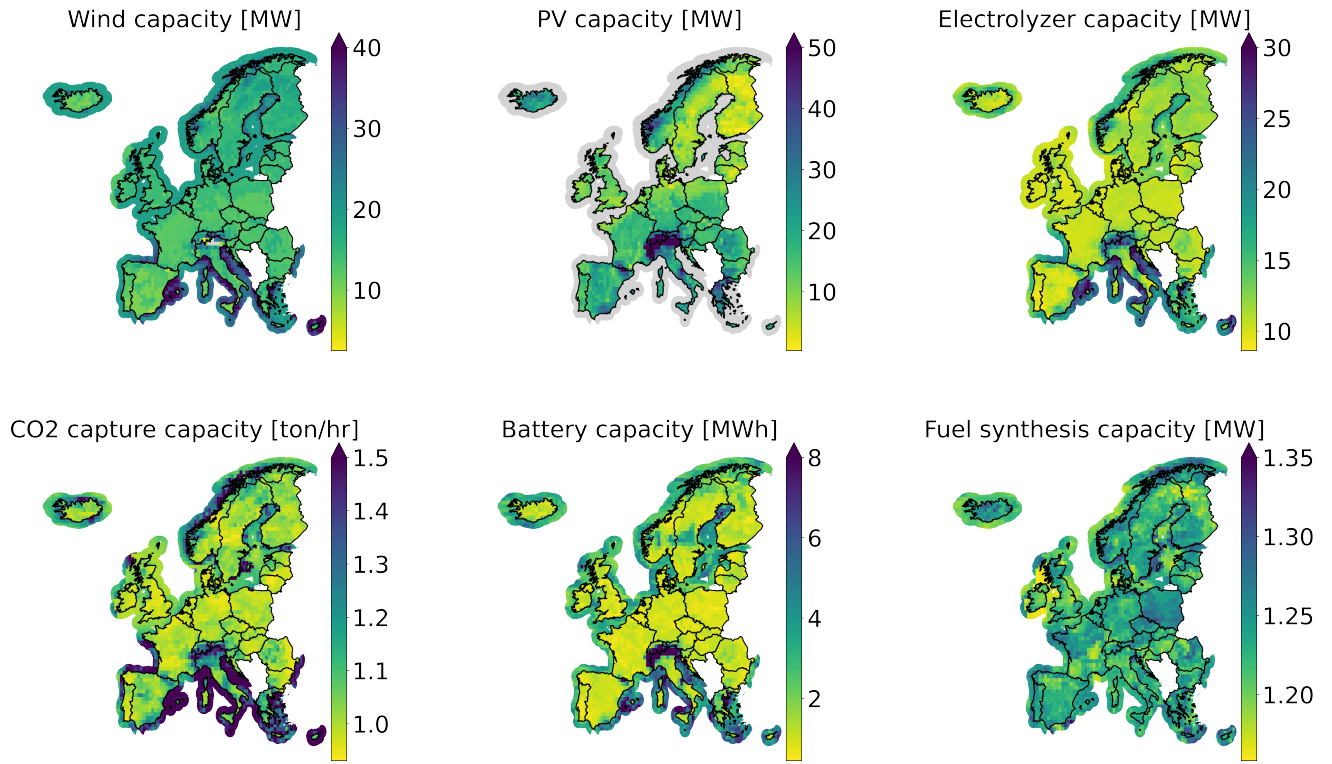
Figure 9 Installed component capacities as selected by the optimiser at each node.

Figure 11 shows the installed PV capacity as share of total installed renewable electricity generation, i.e. from PV and wind power. This map shows the favourable hybrid PV/wind setup due to its flexibility to even out fluctuations of only one renewable electricity generation type.

9 Storage discharge times

Battery, H_2, and CO_2 storage capacities vary significantly across evaluation nodes. Figure 10 represents the optimized storage capacities at all locations given as the duration of discharge time (full depletion) at base load and rated fuel production capacities.
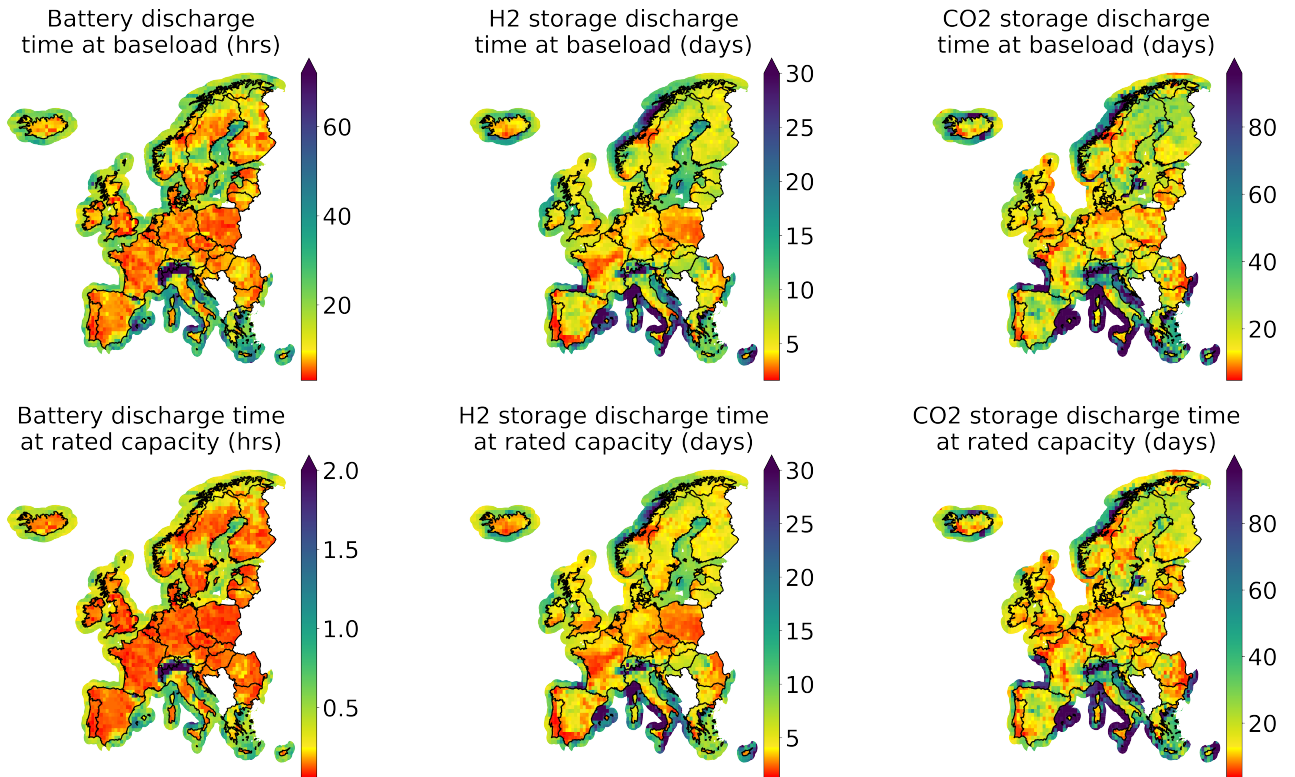
Figure 10 Storage component capacities as selected by the optimiser at each node. The capacities are represented as the discharge time of each component both under base load and also under full rated fuel production capacity rates.

The battery base load represents the electricity required to run only the fuel synthesis process at 80% of rated capacity and no concurrent H_2 production or CO_2 capture. Across all locations, the median discharge time is 12 hours and 80% can sustain base load operation entirely by the battery for up to 24 hours. Battery discharge at rated capacity represents the scenario in which electricity is supplied entirely by the battery for fuel synthesis, H_2 production, and CO_2 capture all running at full capacity simultaneously. This scenario is implausible in almost every case given the discharge power constraint of the battery, but nevertheless indicates the capacity of the battery in relation to the electricity demand of the plant running at full capacity.

H_2 and CO_2 storage capacity are represented as the time it would take for either to discharge from completely full to completely empty at both the rated fuel production capacity of the plant and the base load capacity. The median durations in which base load plant operation could be sustained by stored H_2 and CO_2 are 6 days and 20 days, respectively. In locations where wind and/or PV capacity factors are low, CO_2 storage helps to decouple DAC component sizing from wind and PV sizing. In over 99% of locations, CO_2 storage can sustain base load plant operation without running DAC for one week or longer.

10 Curtailment of electricity

We have modelled PtL-SAF production sites as stand-alone plants that are not connected to the electricity grid. Figure 12 shows the share of annual electricity generation being curtailed. This electricity could potentially generate additional revenues if the plant were to be connected to the grid or some other electricity-consuming process.

11 Domestic PtL-SAF cost production curves

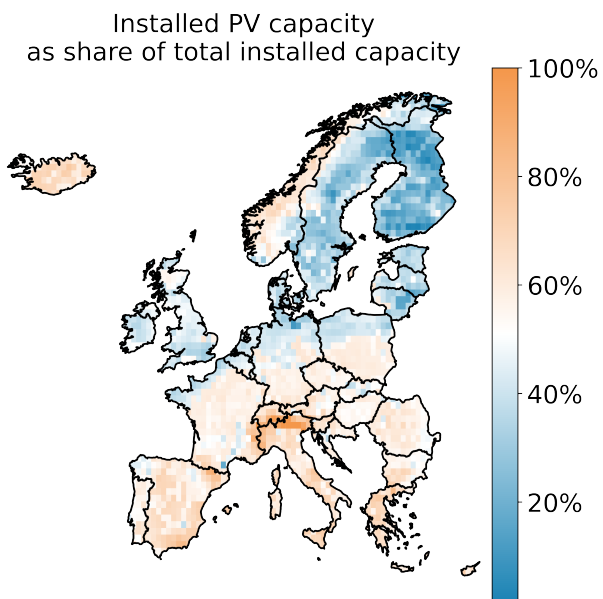Figures 13 and 14 show the domestic cost production curves for all EU32 countries.

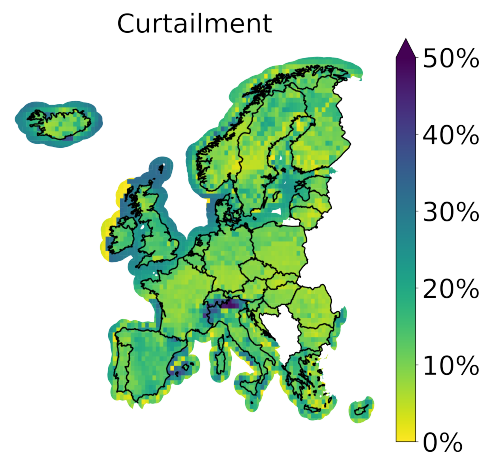**Figure 11 Optimised share of electricity generation capacity from PV.** All other generation capacity comes from wind.

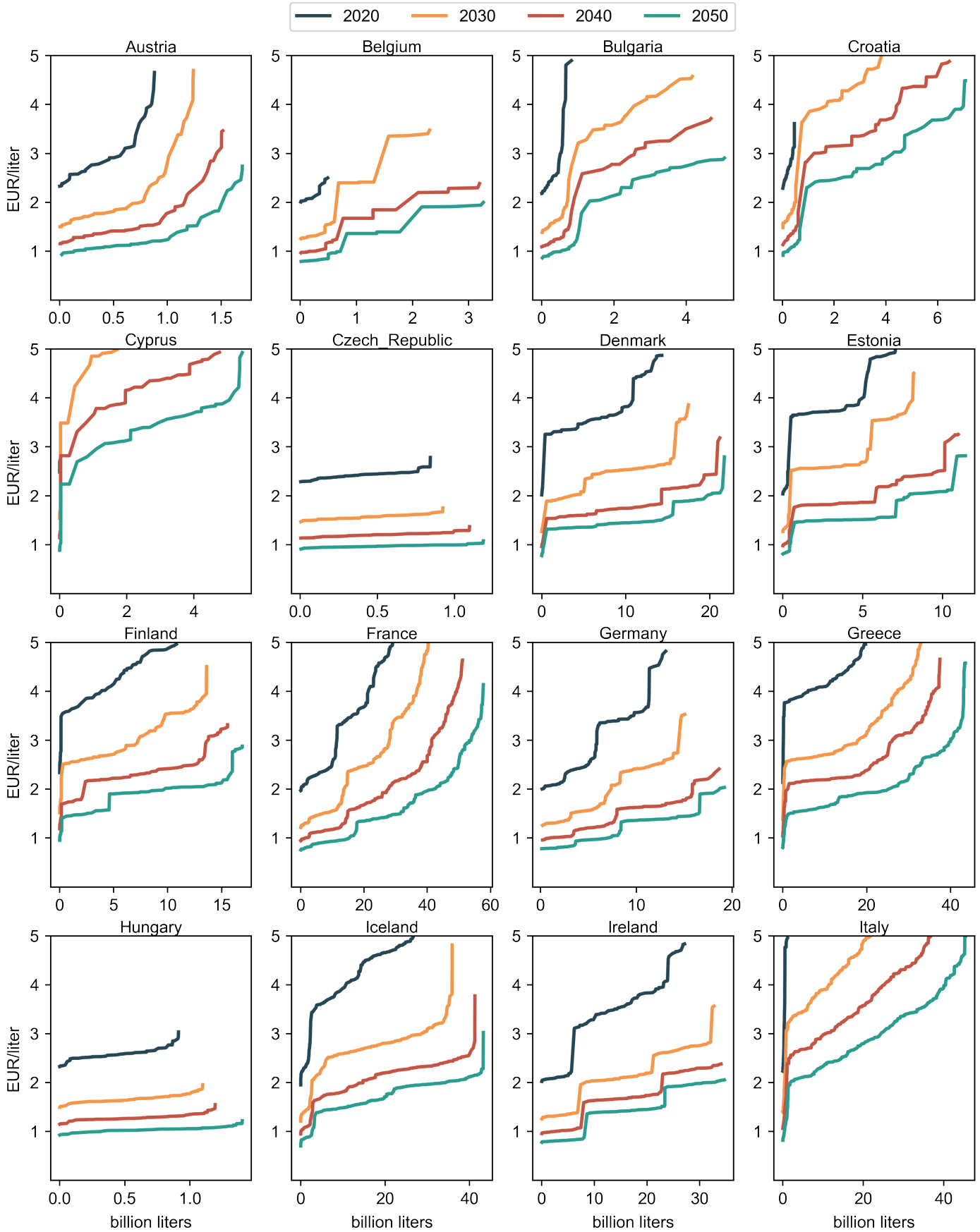**Figure 12 Annual electricity generation curtailment.**

Figure 13 Country-specific cost production curves (1/2) if sparsely vegetated areas, pastures and offshore areas are made available for fuel production.
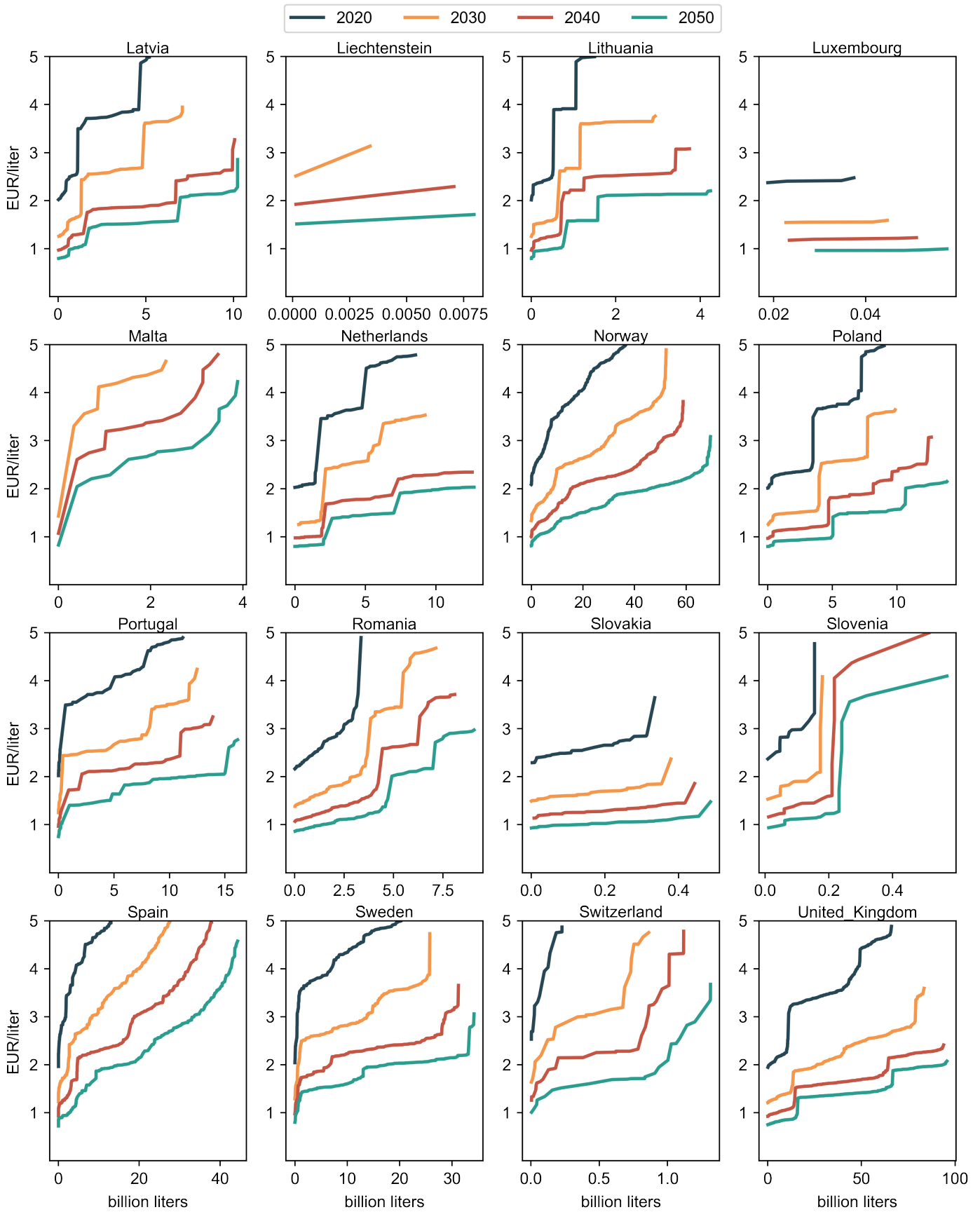
Figure 14 Country-specific cost production curves (2/2) if sparsely vegetated areas, pastures and offshore areas are made available for fuel production.

12 Green premium and GHG abatement costs of PtL-SAF production

To quantify the impact of increased fuel prices on the end customer, we present a case study investigating the effect of blending mandates on ticket prices. The green premium of a ticket, GP_{ticket}, reflected in Equation 28, is given as the increase of the cost due to the use of PtL-SAF relative to the hypothetical cost if fossil fuels were to be used in some future year, N. Costs, given in Equation 29, can be represented as the sum of fuel costs and non-fuel costs, NFC, where fuel costs are the product of LCOF and fuel quantity, FQ_N. Fuel quantity in hypothetical future year, N, which is given in Equation 30, reduces as a function of annual fuel efficiency improvements, η, assumed to be equal to 1.5% per year[30] in both the PtL-SAF fuel blend and fossil fuel cases. The LCOF of a blend of fossil jet fuel and PtL-SAF, $LCOF_{mix}$, with some fraction of PtL-SAF, f_{PtL}, is given in Equation 31.

$$GP_{ticket} = \frac{costs_{blend}}{costs_{fossil}} - 1 \tag{28}$$

$$costs = FQ_N \cdot LCOF + NFC \tag{29}$$

$$FQ_N = FQ_0(1-\eta)^N \tag{30}$$

$$LCOF_{mix} = f_{PtL} * LCOF_{PtL} + (1 - f_{PtL}) * LCOF_{fossil} \tag{31}$$

It is assumed that the current share of fuel costs on total costs of ownership of an airline is 25% and non-fuel costs remain constant in future years, resulting in the equalities given in Equation 32.

$$NFC = 3 \cdot FQ_0 \cdot LCOF_0 = 3 \cdot FQ_0 \cdot LCOF_{fossil,2020} \tag{32}$$

Combining Equations 28, 29, 30, and 32, leads to Equation 33, which reduces to Equation 34 with the assumption that the cost of fossil fuel in future years remains unchanged from the 2020 level.

$$GP_{ticket} = \frac{FQ_0(1-\eta)^N \cdot LCOF_{mix,N} + 3 \cdot FQ_0 \cdot LCOF_{fossil,2020}}{FQ_0(1-\eta)^N \cdot LCOF_{fossil,N} + 3 \cdot FQ_0 \cdot LCOF_{fossil,2020}} - 1 \tag{33}$$

$$GP_{ticket} = \frac{(1-\eta)^N \cdot LCOF_{mix} + 3 \cdot LCOF_{fossil}}{(1-\eta)^N \cdot LCOF_{fossil} + 3 \cdot LCOF_{fossil}} - 1 \tag{34}$$

13 Plant cost breakdown

The relative sizes of component capacities are a function of the local wind and PV resources. Thus, the share of installation cost (NPV of CAPEX and OPEX) attributable to each plant component is not fixed. It is possible, however, to generalise the cost share based on the mean for each component. These mean cost shares, as well as 5-95 percentile ranges for all nodes are shown in Figures 15-18. For both onshore and offshore locations, wind turbines represent the largest share of installation costs on average, followed by the electrolyser.

To further illuminate the attribution of costs to plant components, Figure 19 includes the cost breakdown for 11 representative onshore sites in 2050. The costs are represented again as the NPV of CAPEX and OPEX. The sites were sorted by LCOF, and every 10th percentile was selected. The left-most bar represents the site with the lowest LCOF, the next bar represents the site at the 10th percentile of LCOF, and so on. For sites below the 90th percentile of LCOF, there is slight variation in cost breakdown that is primarily due to the balance of wind and PV costs. The two sites representing the 90th percentile of LCOF and the highest LCOF are entirely powered by PV, with the inherent diurnal and seasonal fluctuations in irradiance availability leading to expensive overbuilding, curtailment, and storage buffer. As the wind, PV, and electrolyser costs make up 75% or more of total plant costs for all sites at or below the 30th percentile of LCOF (where plants are more likely to be built), uncertainties related to these costs are most important.
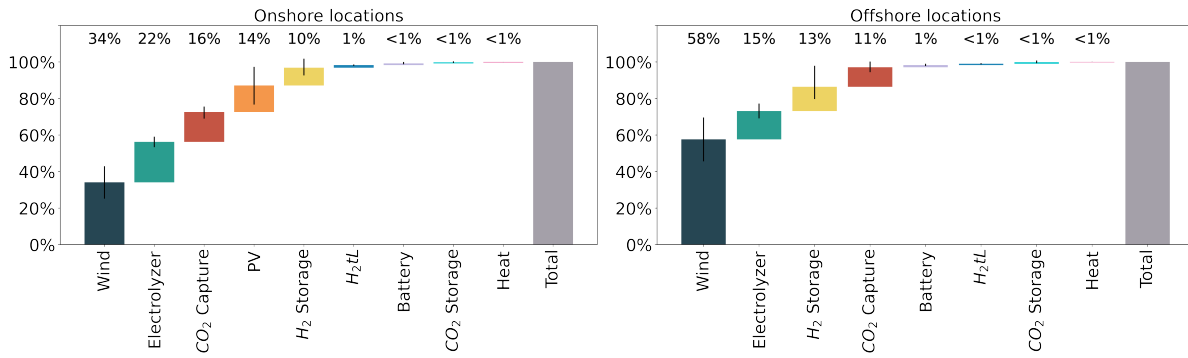
Figure 15 Share of plant cost (NPV of CAPEX and OPEX) from each component in 2020. The coloured bars represent the mean cost share for each component across all evaluation nodes. The black error lines indicate the range of the 5th and 95th percentile of the component cost shares.
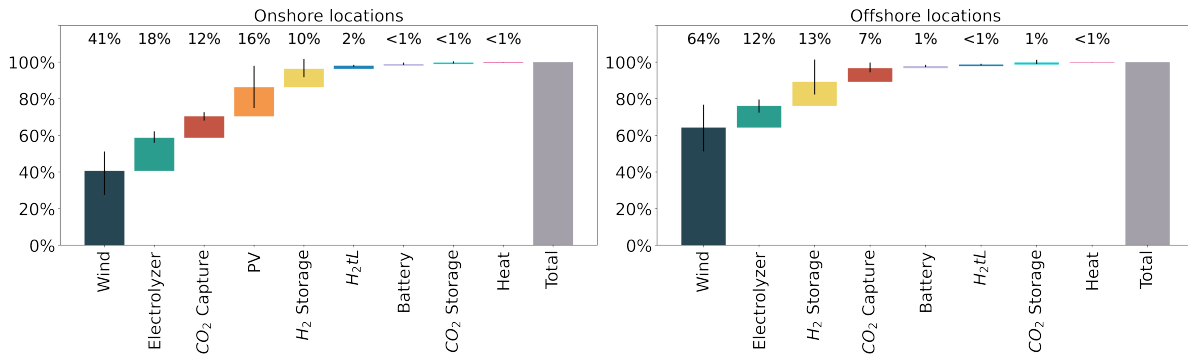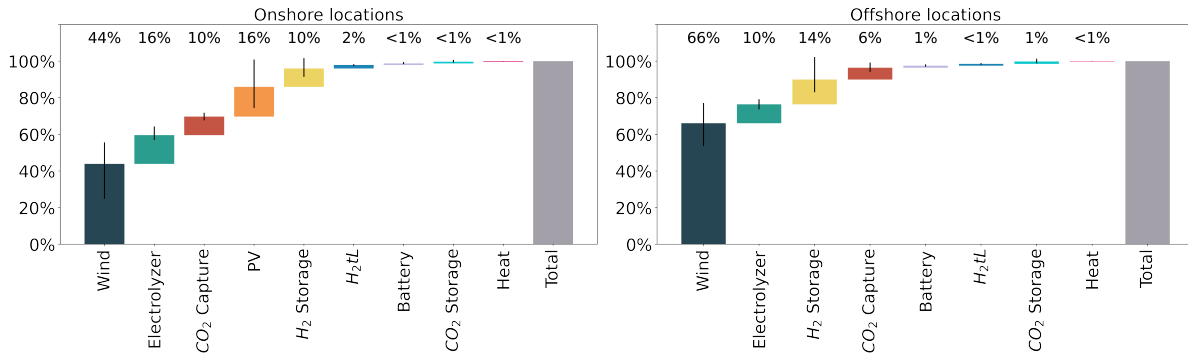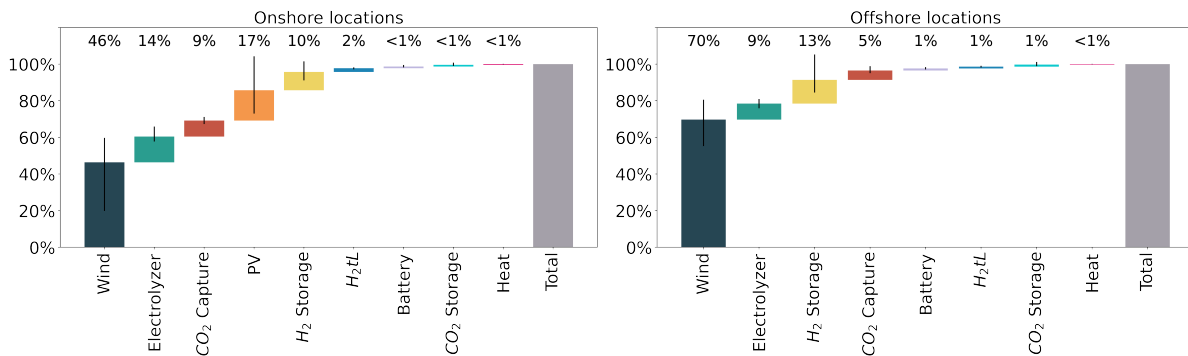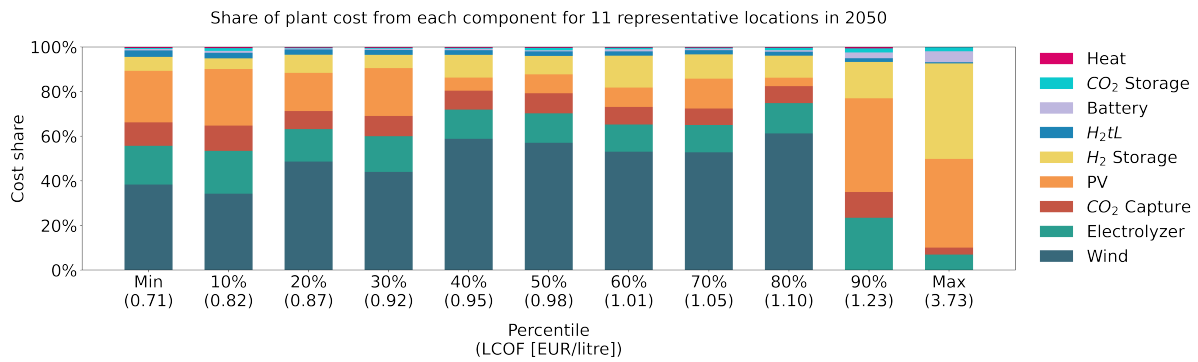

Figure 16 Share of plant cost (NPV of CAPEX and OPEX) from each component in 2030. The coloured bars represent the mean cost share for each component across all evaluation nodes. The black error lines indicate the range of the 5th and 95th percentile of the component cost shares.

Figure 17 Share of plant cost (NPV of CAPEX and OPEX) from each component in 2040. The coloured bars represent the mean cost share for each component across all evaluation nodes. The black error lines indicate the range of the 5th and 95th percentile of the component cost shares.

Figure 18 Share of plant cost (NPV of CAPEX and OPEX) from each component in 2050. The coloured bars represent the mean cost share for each component across all evaluation nodes. The black error lines indicate the range of the 5th and 95th percentile of the component cost shares.

Figure 19 Share of plant cost (NPV of CAPEX and OPEX) from each component at 11 representative sites in 2050. The sites chosen are those at every 10th percentile of LCOF. The bars represent cost shares in locations for the following countries (from left to right): Iceland, Greece, Romania, Poland, Poland, Sweden, Lithuania, France, Sweden, Greece, Italy.

14 Country-level LCOF maps

In the following figures, the geographic and temporal variations in LCOF are represented at a country level.
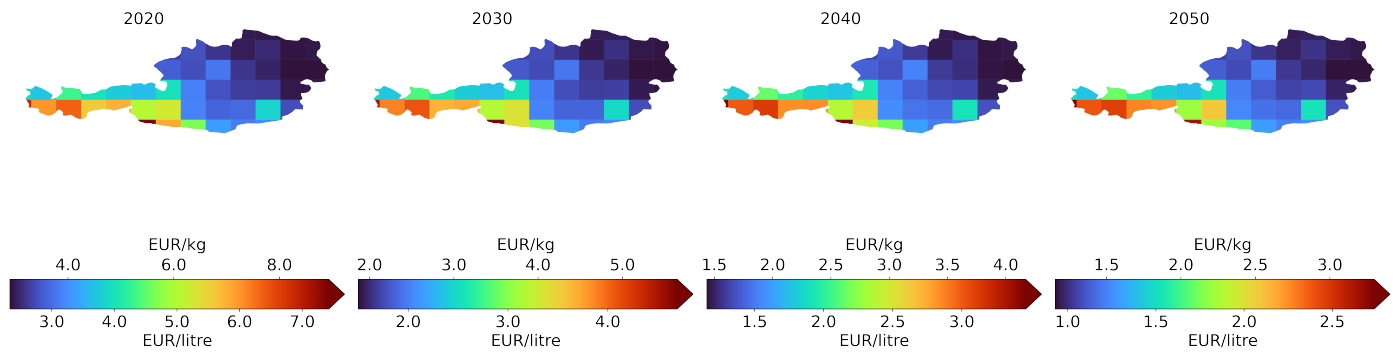
Figure 20 PtL-SAF production costs in Austria for 2020, 2030, 2040, and 2050.
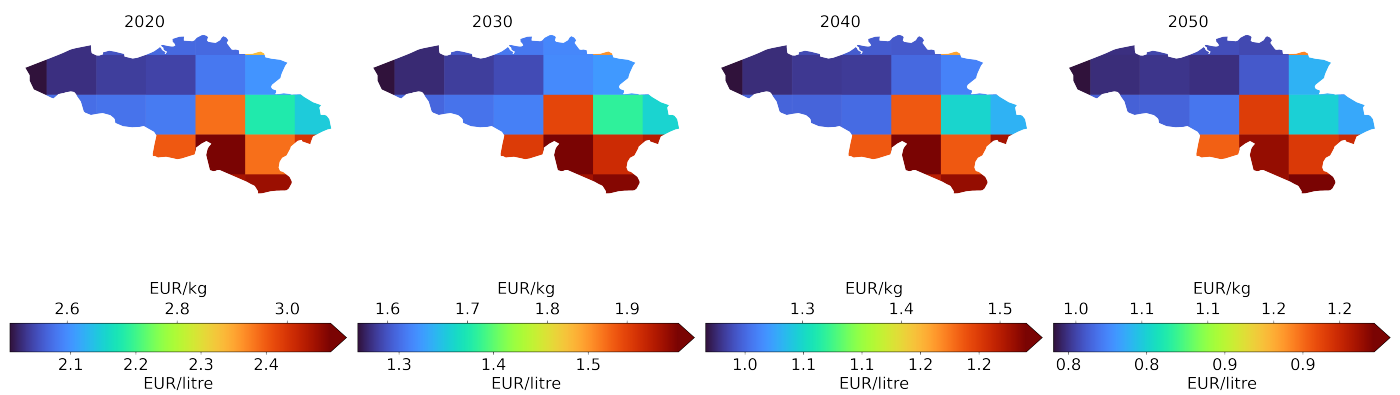
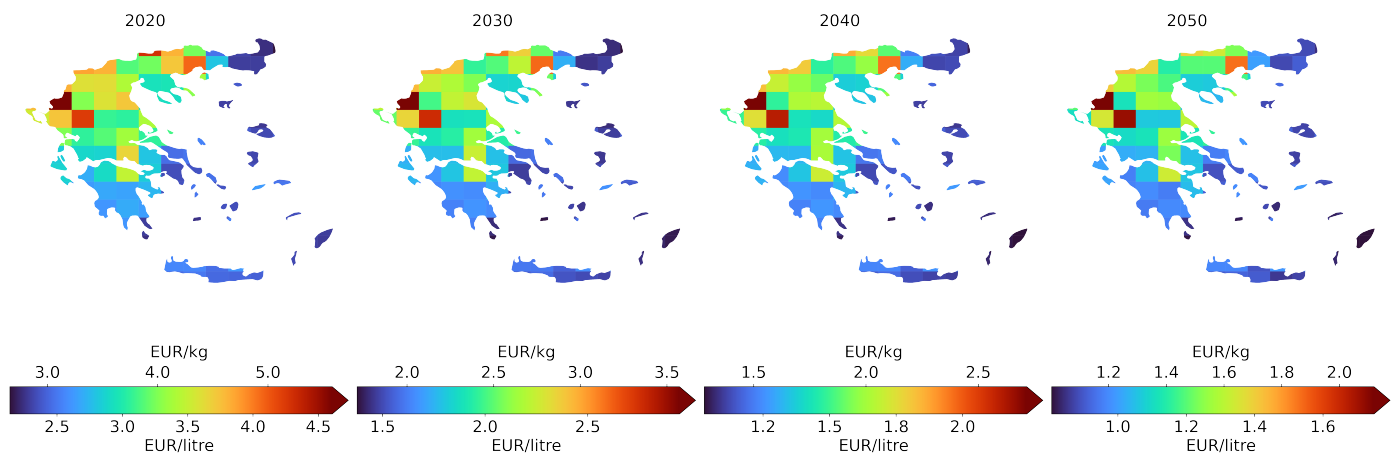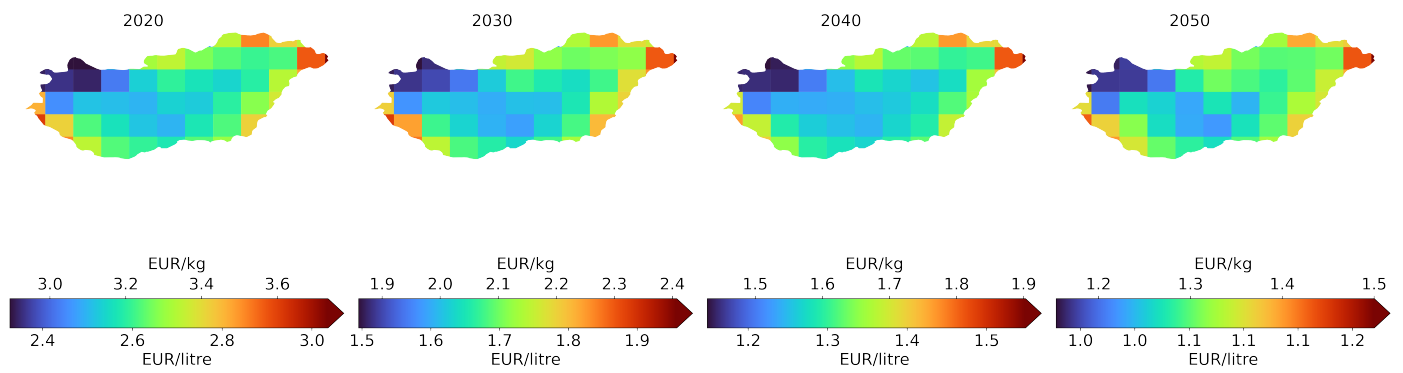**Figure 21** PtL-SAF production costs in Belgium for 2020, 2030, 2040, and 2050.
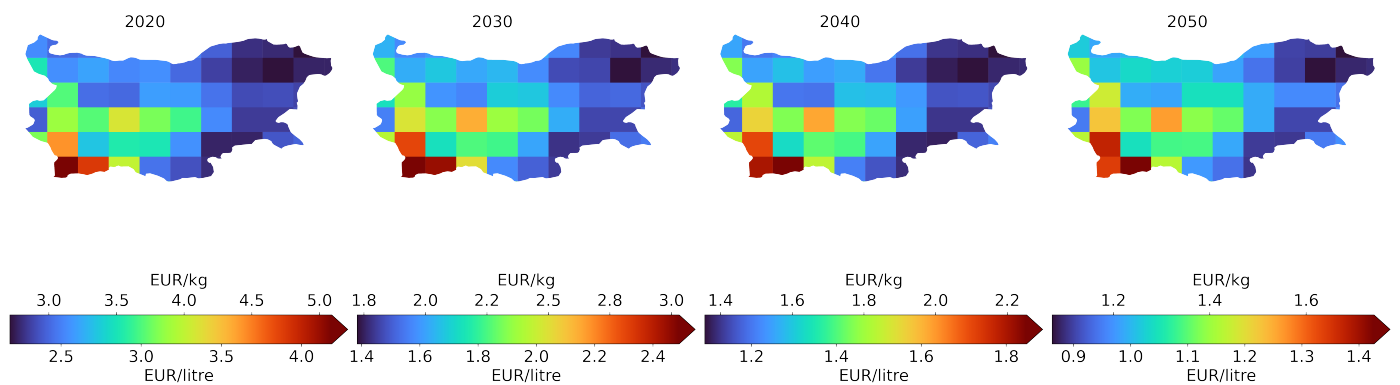
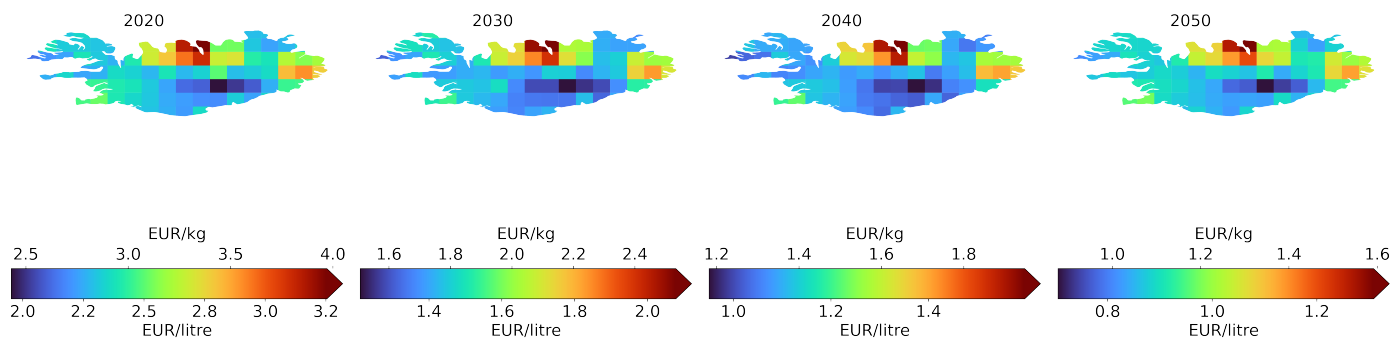**Figure 22** PtL-SAF production costs in Bulgaria for 2020, 2030, 2040, and 2050.
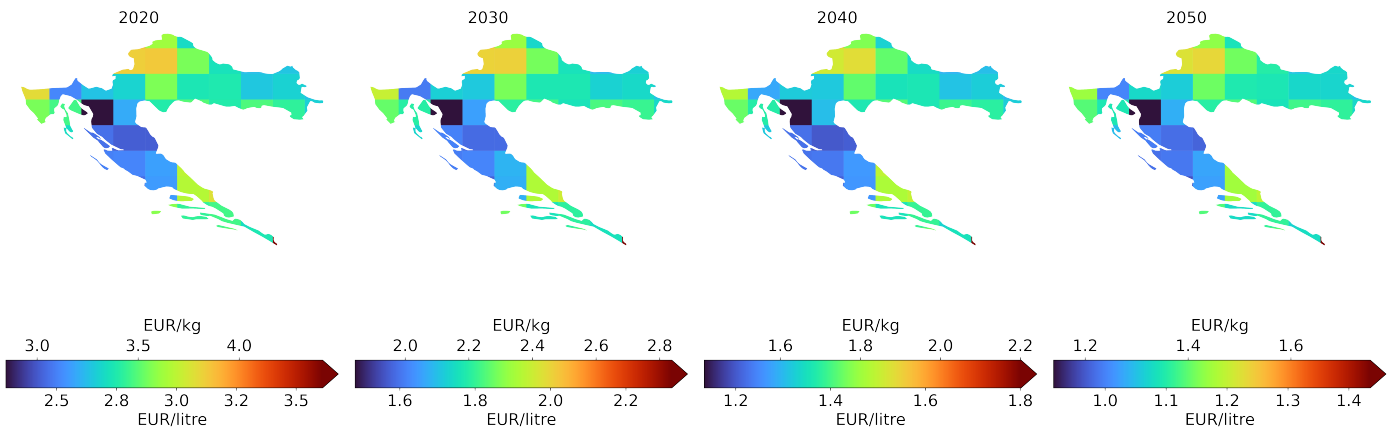
Figure 23 PtL-SAF production costs in Croatia for 2020, 2030, 2040, and 2050.
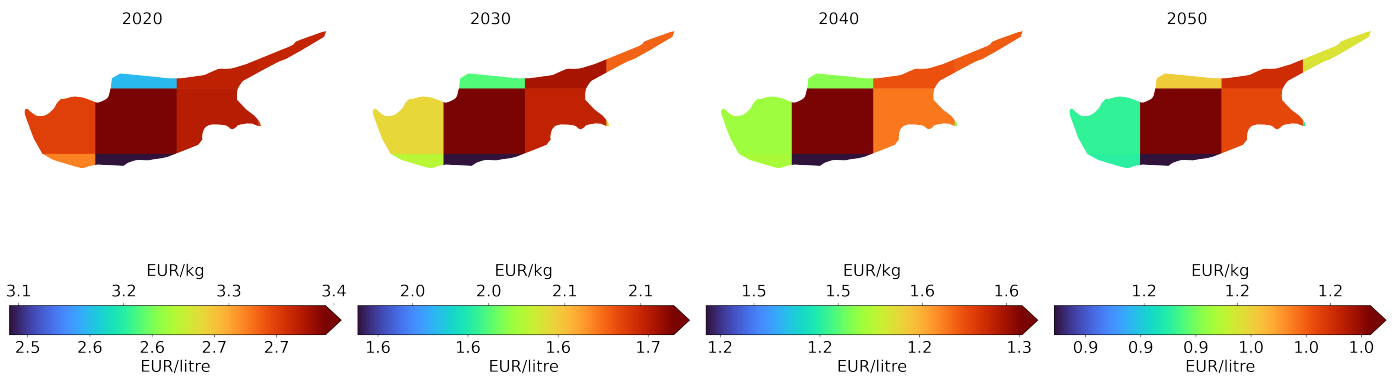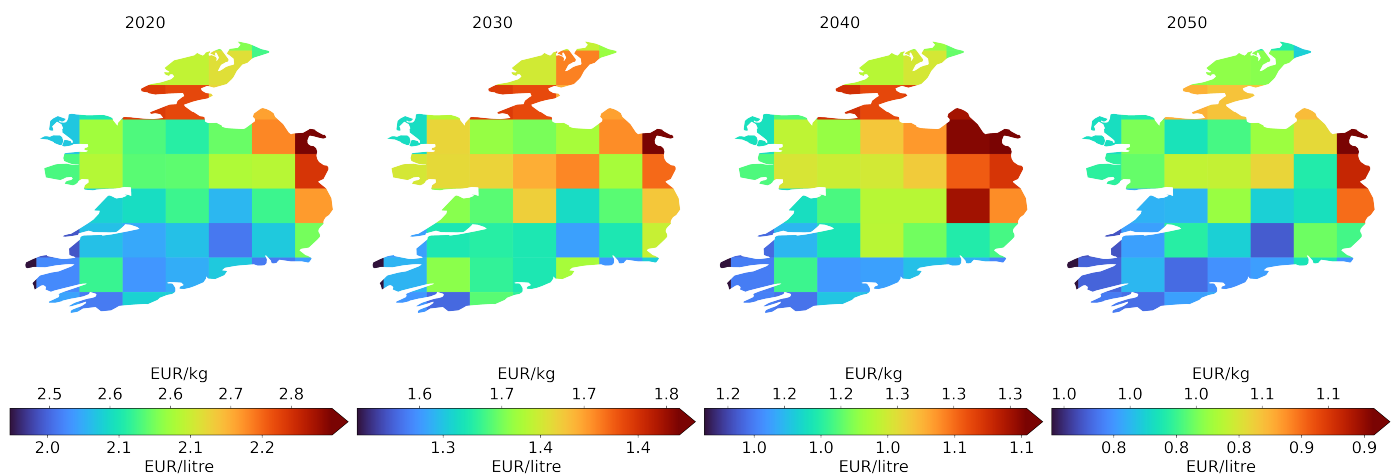

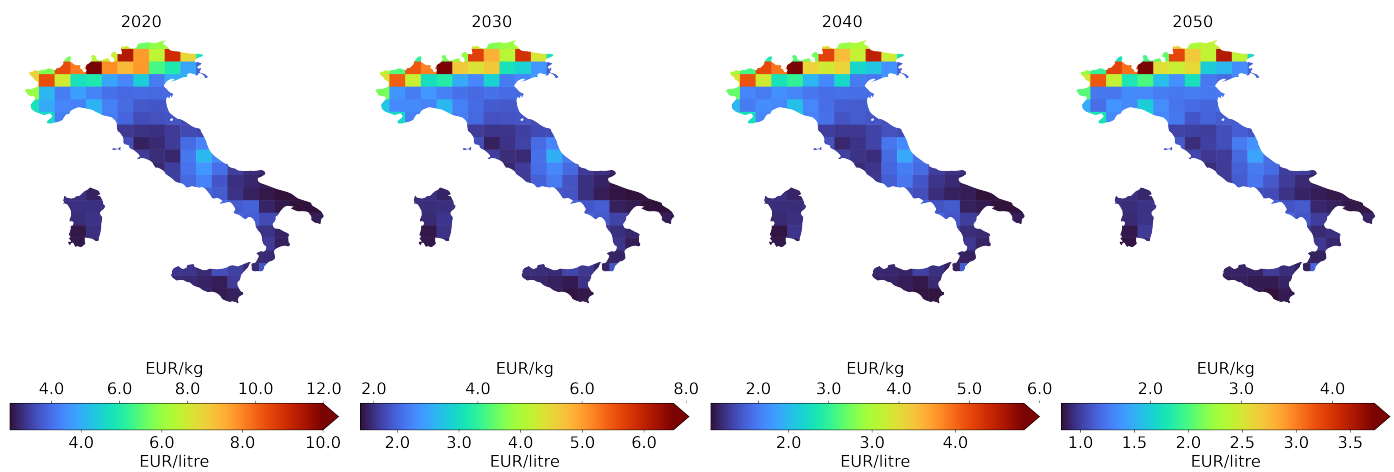**Figure 24** PtL-SAF production costs in Cyprus for 2020, 2030, 2040, and 2050.
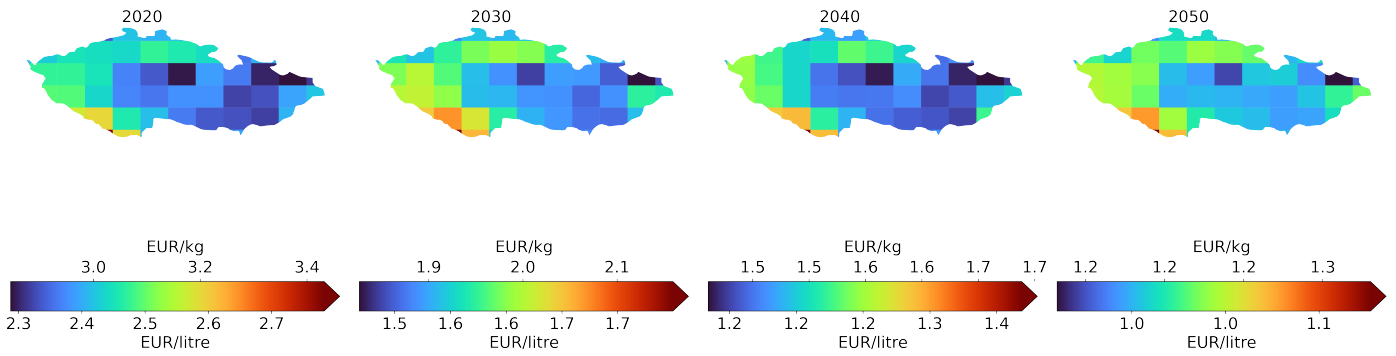
Figure 25 PtL-SAF production costs in Czech Republic for 2020, 2030, 2040, and 2050.
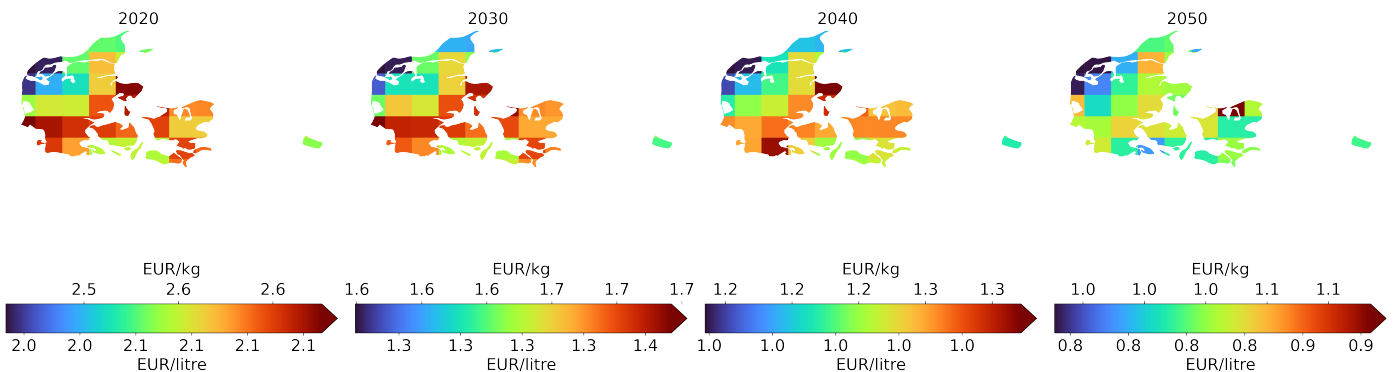
Figure 26 PtL-SAF production costs in Denmark for 2020, 2030, 2040, and 2050.
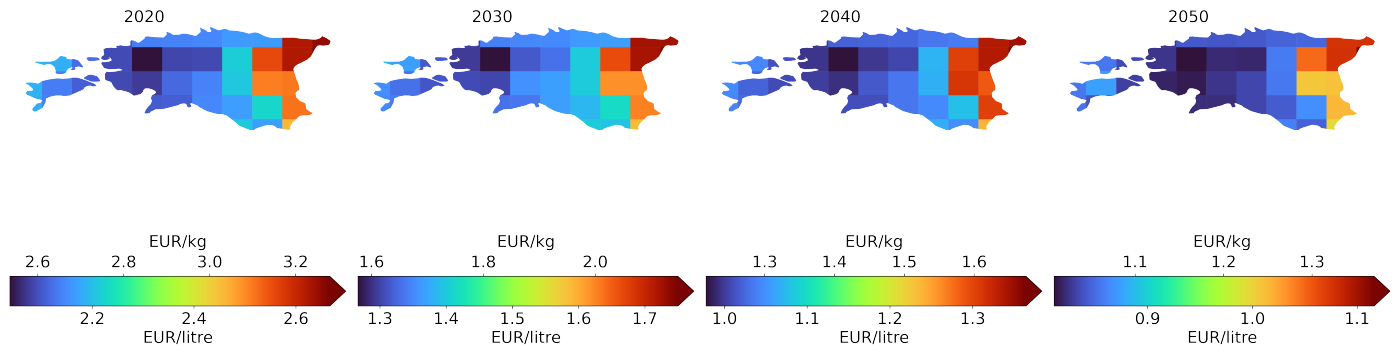
Figure 27 PtL-SAF production costs in Estonia for 2020, 2030, 2040, and 2050.
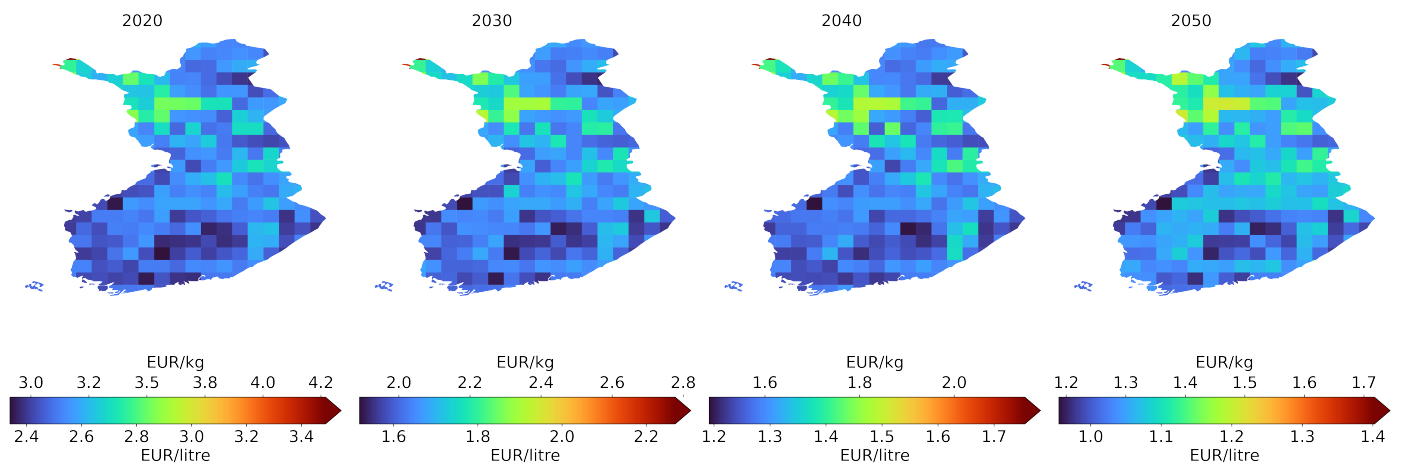
Figure 28 PtL-SAF production costs in Finland for 2020, 2030, 2040, and 2050.
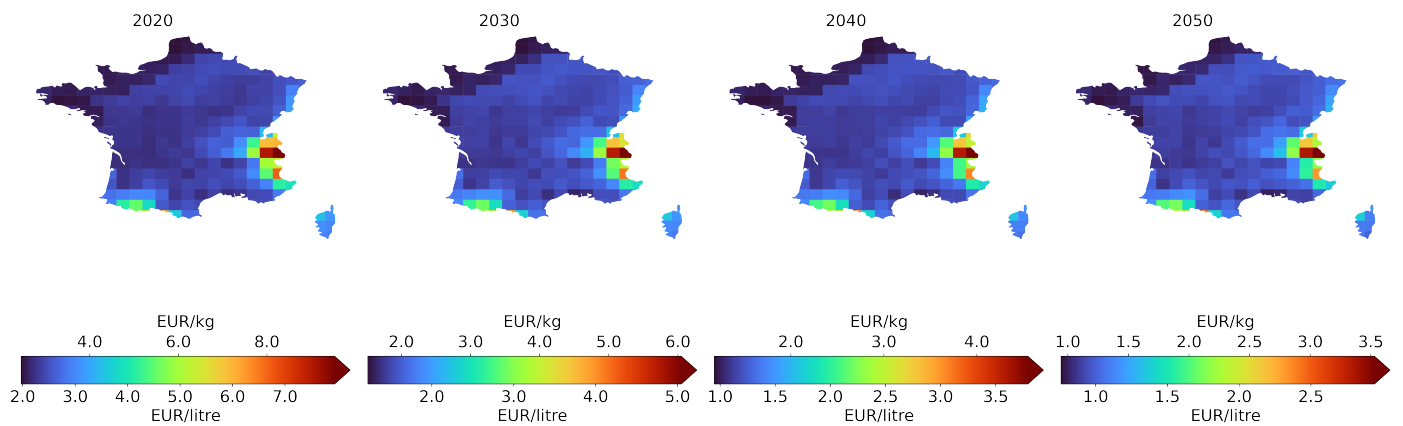
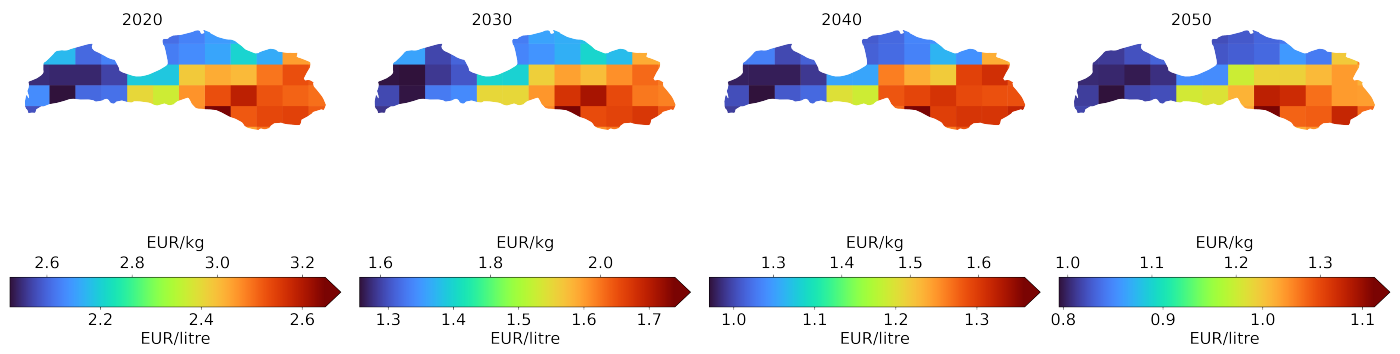**Figure 29** PtL-SAF production costs in France for 2020, 2030, 2040, and 2050.
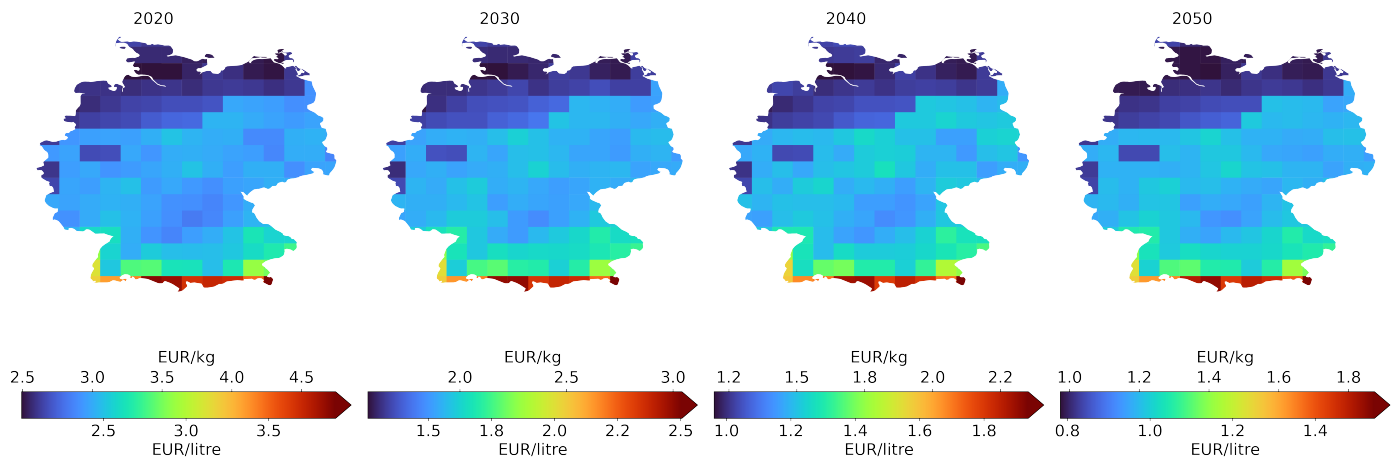
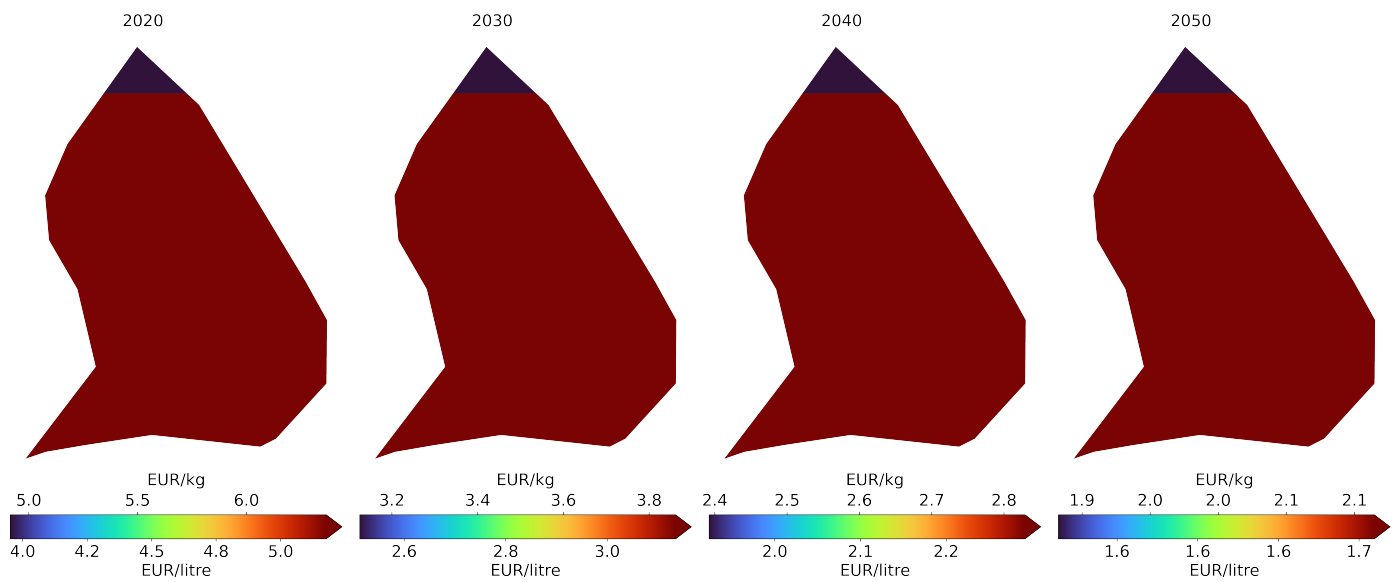**Figure 30** PtL-SAF production costs in Germany for 2020, 2030, 2040, and 2050.

Figure 31 PtL-SAF production costs in Greece for 2020, 2030, 2040, and 2050.

Figure 32 PtL-SAF production costs in Hungary for 2020, 2030, 2040, and 2050.

Figure 33 PtL-SAF production costs in Iceland for 2020, 2030, 2040, and 2050.

Figure 34 PtL-SAF production costs in Ireland for 2020, 2030, 2040, and 2050.

Figure 35 PtL-SAF production costs in Italy for 2020, 2030, 2040, and 2050.

Figure 36 PtL-SAF production costs in Latvia for 2020, 2030, 2040, and 2050.

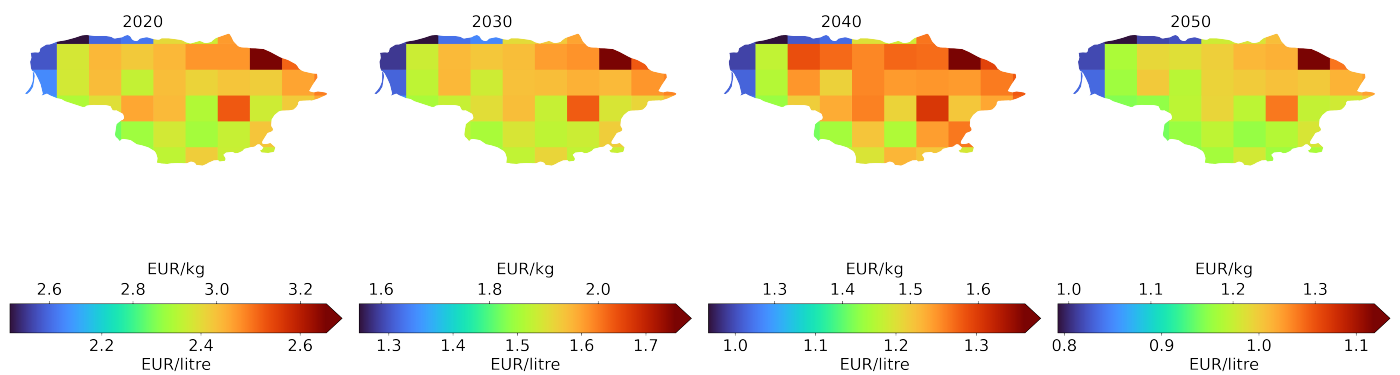**Figure 37** PtL-SAF production costs in Liechtenstein for 2020, 2030, 2040, and 2050.

Figure 38 PtL-SAF production costs in Lithuania for 2020, 2030, 2040, and 2050.
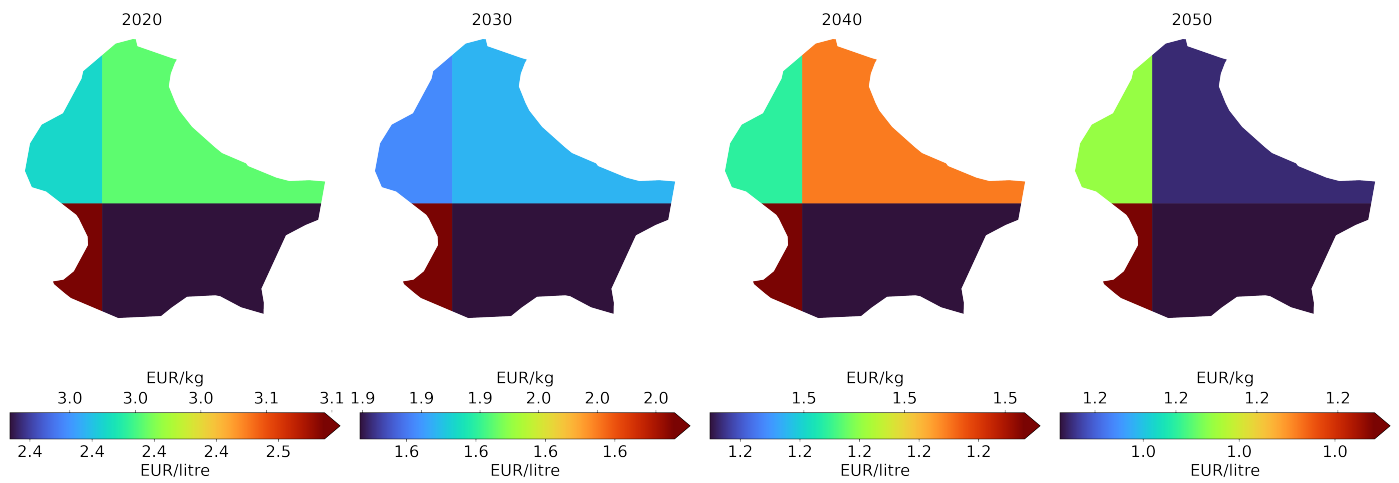
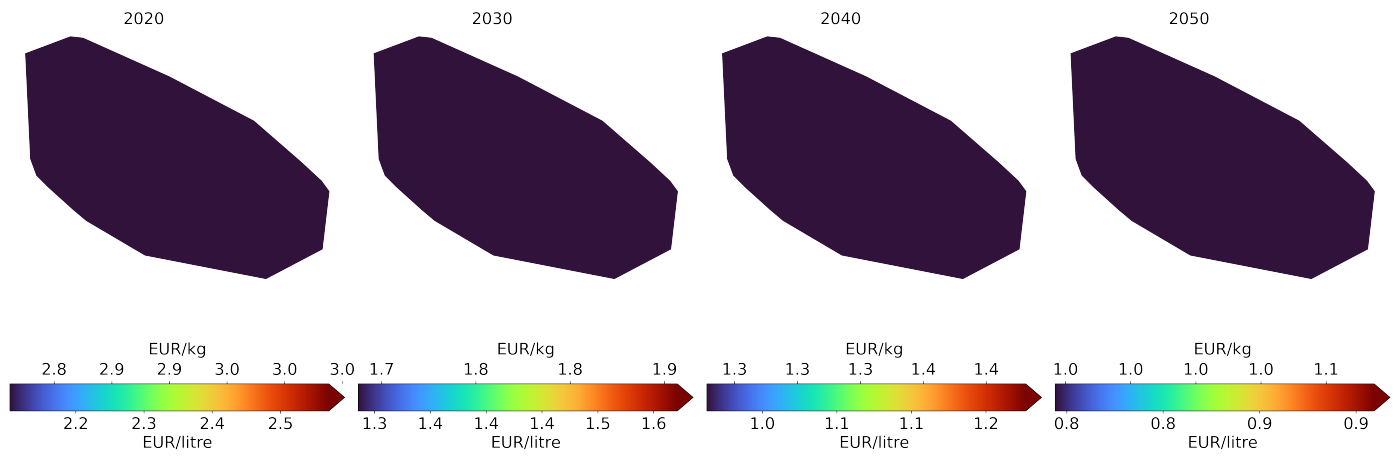**Figure 39** PtL-SAF production costs in Luxembourg for 2020, 2030, 2040, and 2050.

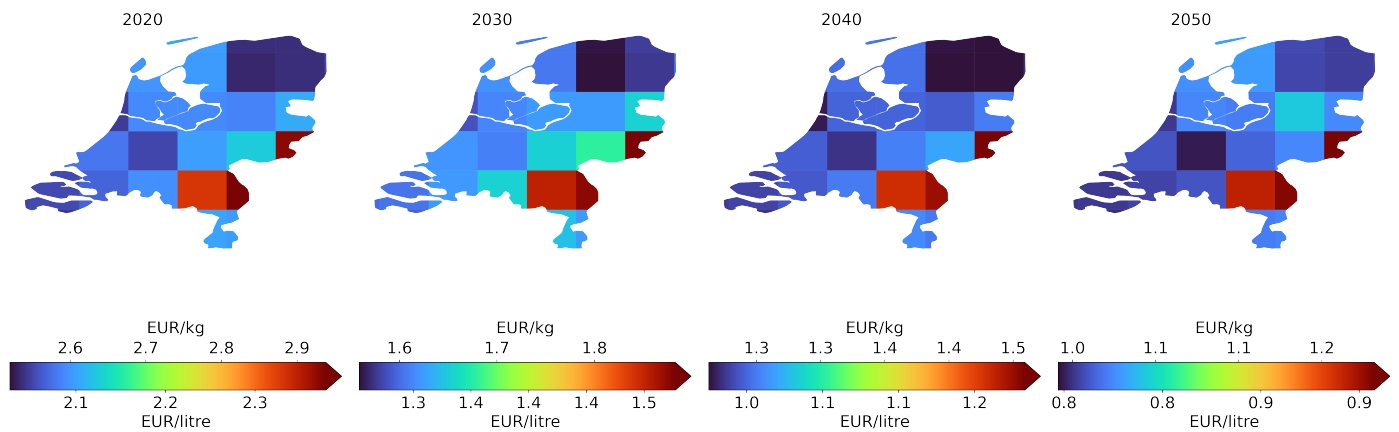**Figure 40** PtL-SAF production costs in Malta for 2020, 2030, 2040, and 2050.

Figure 41 PtL-SAF production costs in Netherlands for 2020, 2030, 2040, and 2050.
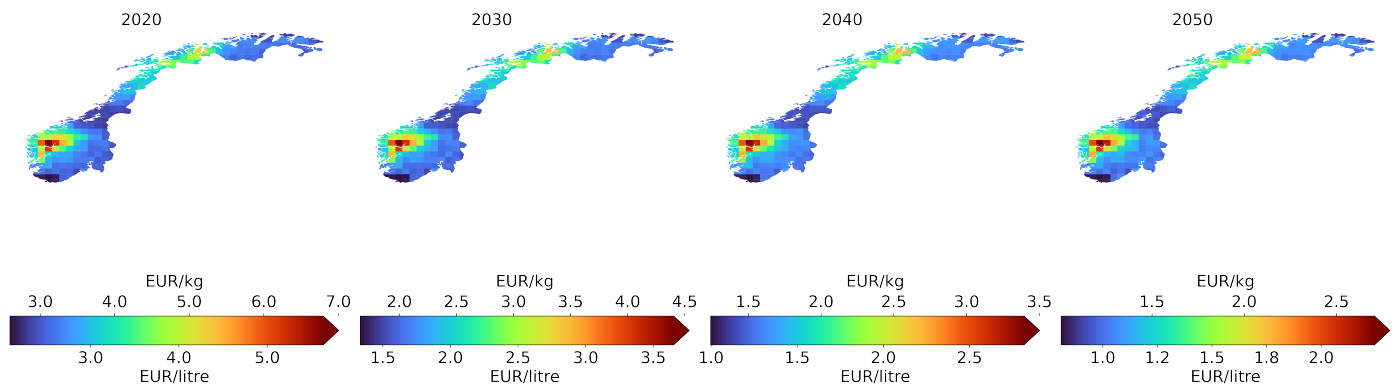
Figure 42 PtL-SAF production costs in Norway for 2020, 2030, 2040, and 2050.
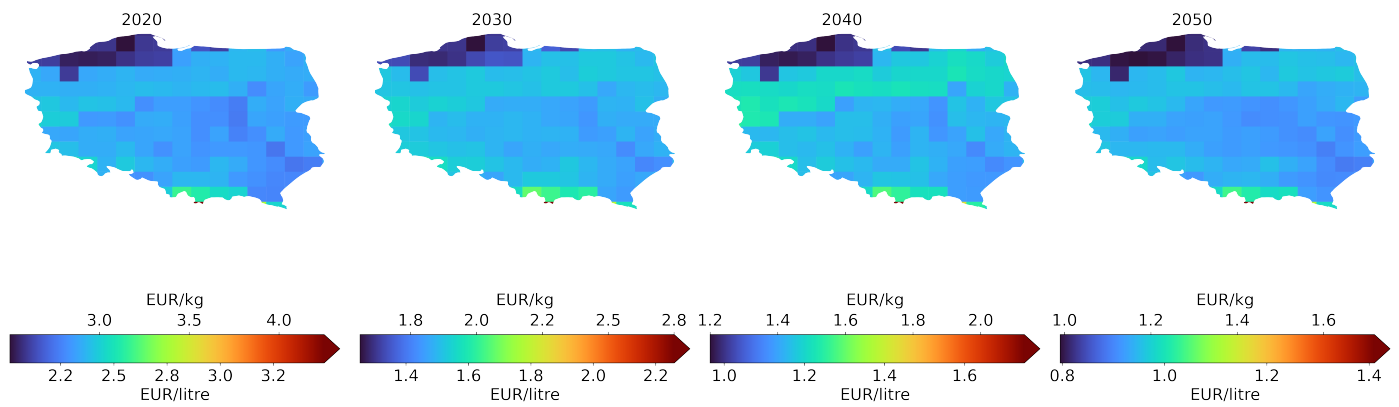

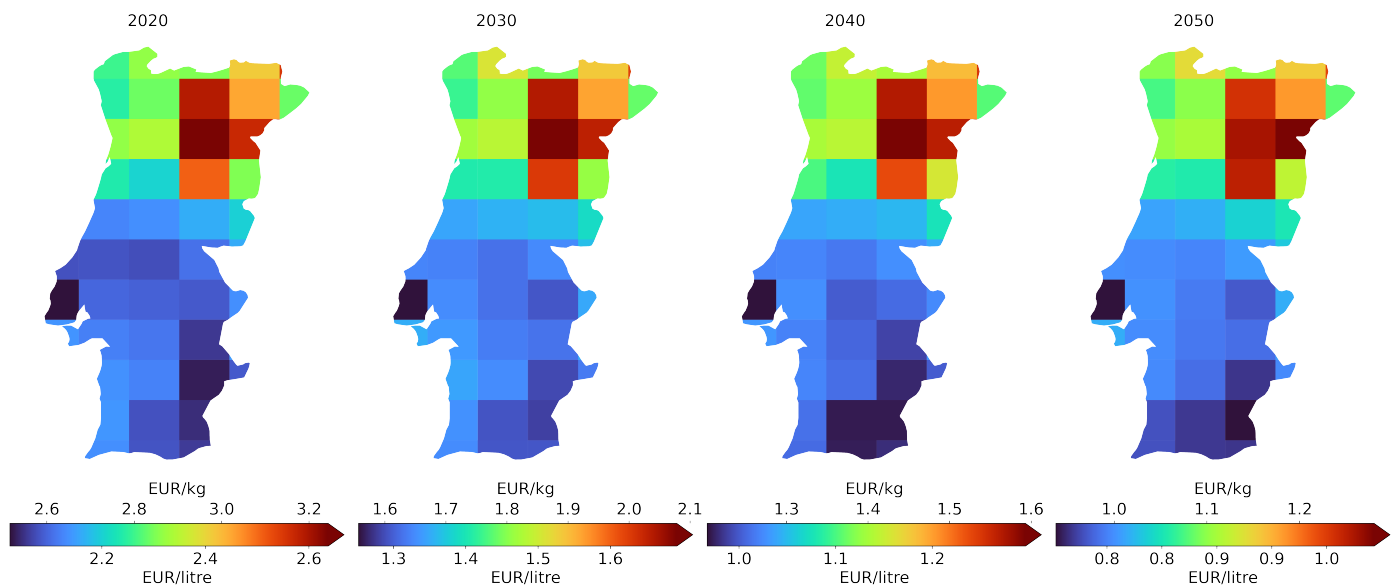Figure 43 PtL-SAF production costs in Poland for 2020, 2030, 2040, and 2050.

Figure 44 PtL-SAF production costs in Portugal for 2020, 2030, 2040, and 2050.
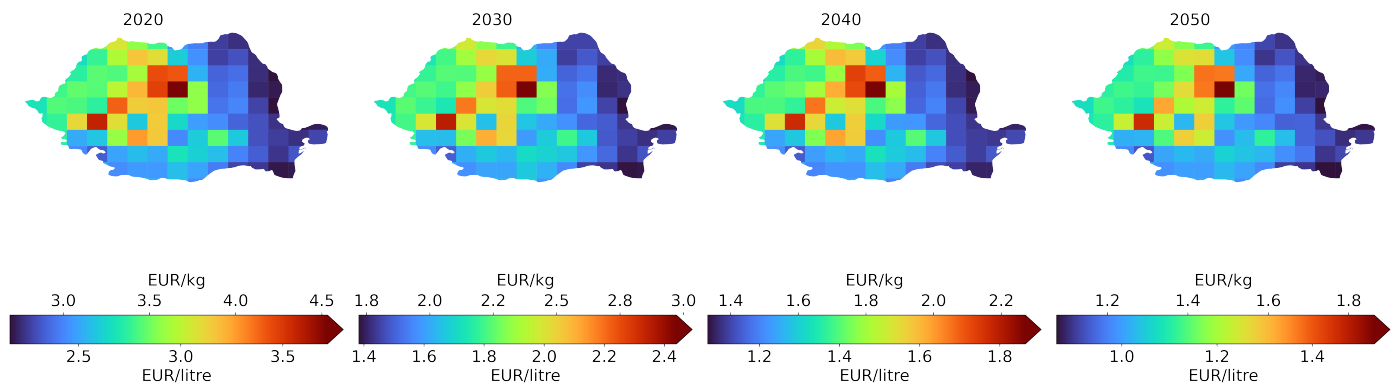
Figure 45 PtL-SAF production costs in Romania for 2020, 2030, 2040, and 2050.
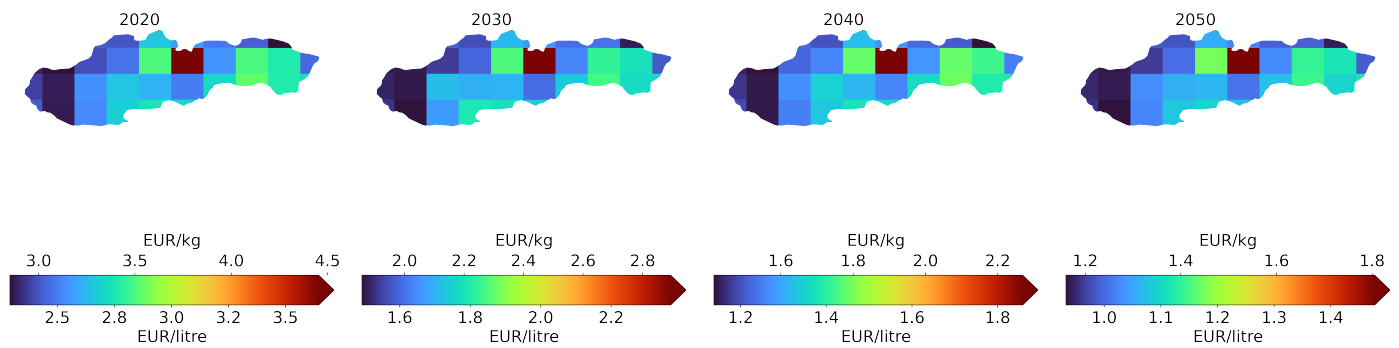

Figure 46 PtL-SAF production costs in Slovakia for 2020, 2030, 2040, and 2050.

Figure 47 PtL-SAF production costs in Slovenia for 2020, 2030, 2040, and 2050.

Figure 48 PtL-SAF production costs in Spain for 2020, 2030, 2040, and 2050.

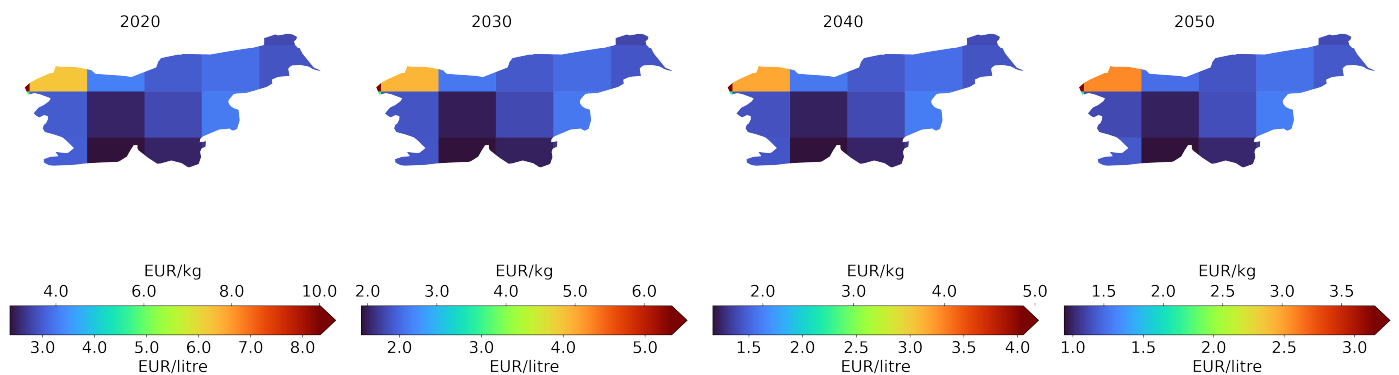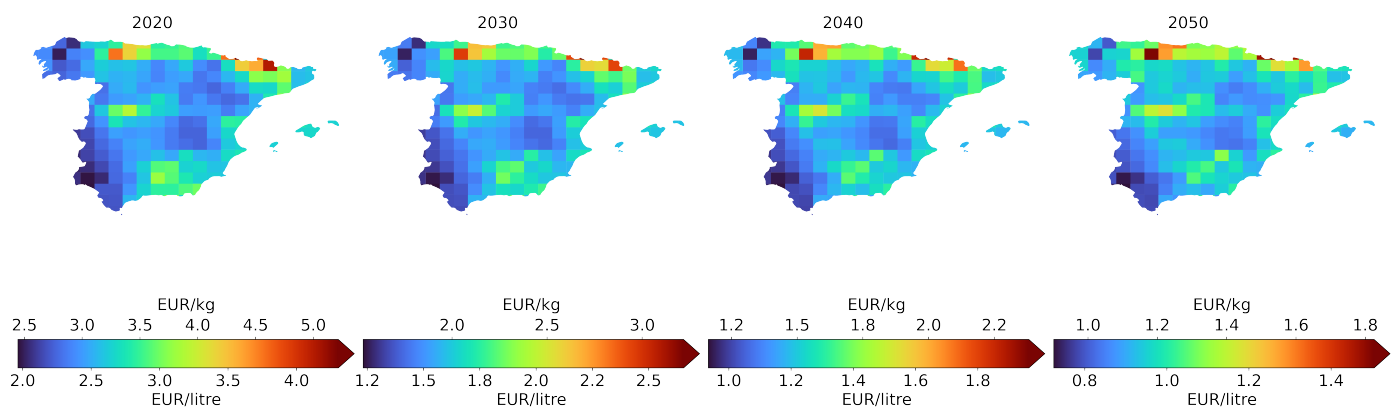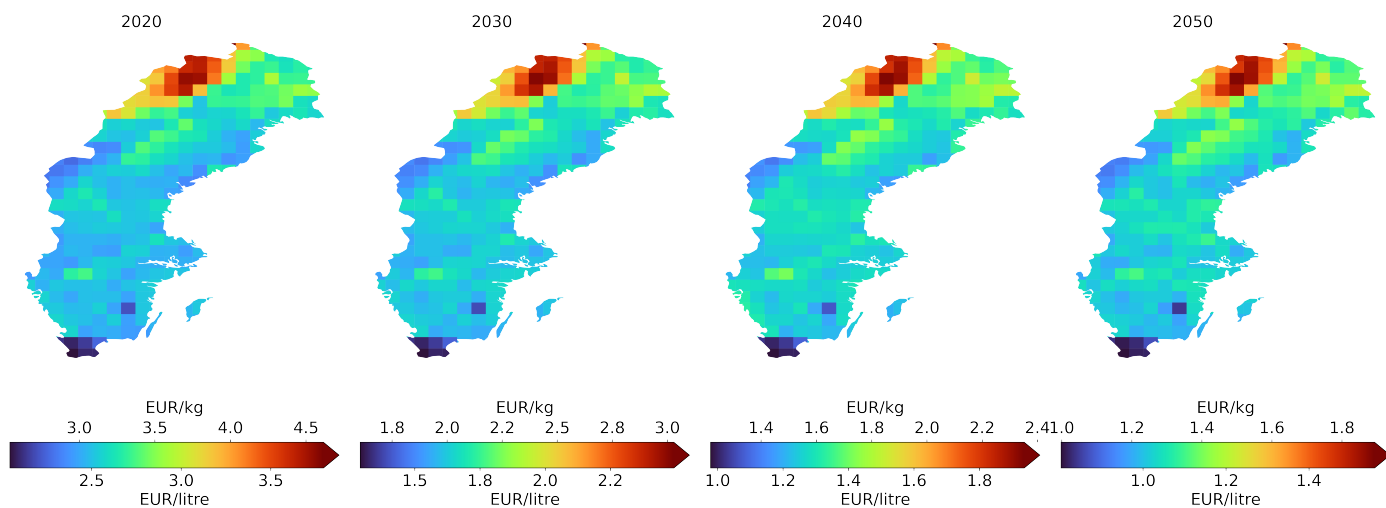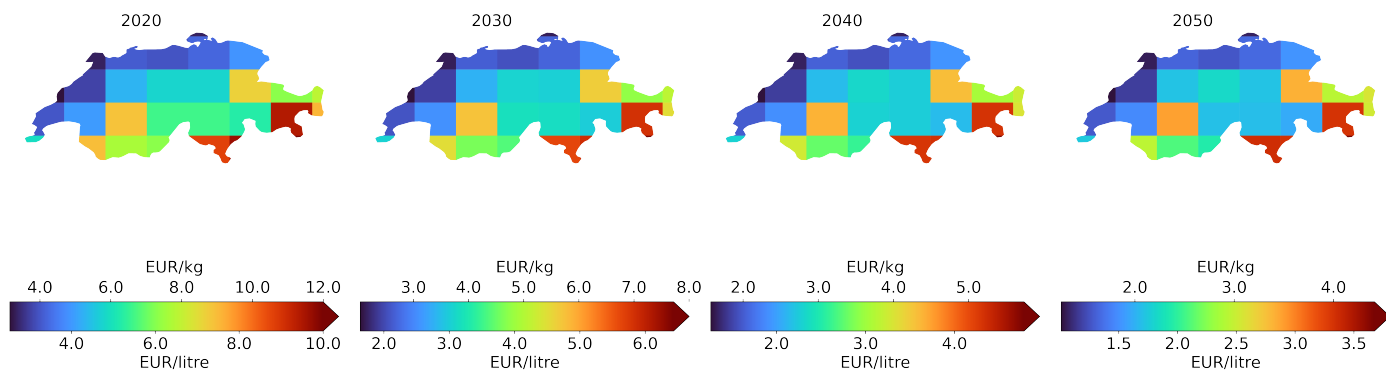**Figure 49** PtL-SAF production costs in Sweden for 2020, 2030, 2040, and 2050.

Figure 50 PtL-SAF production costs in Switzerland for 2020, 2030, 2040, and 2050.
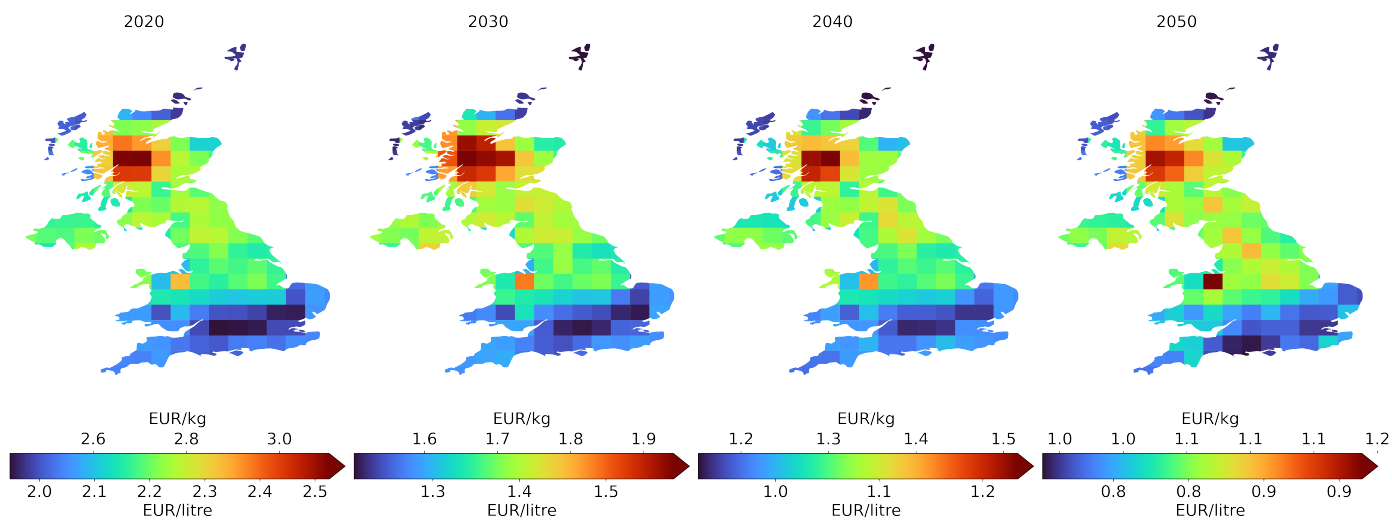

Figure 51 PtL-SAF production costs in United Kingdom for 2020, 2030, 2040, and 2050.

References

1 Engineering ToolBox, *Fuels - Densities and Specific Volume*, 2013, `https://www.engineeringtoolbox.com/fuels-densities-specific-volumes-d{_}166.html`.

2 UN Stats, *Conversion Factors (Net Calorific Values)*, United nations technical report, 2014.

3 International Civil Aviation Organization (ICAO), *2019 Environmental Report: Aviation and Environment - Destination Green, The Next Chapter*, International Civil Aviation Organization, 2019.

4 E. Vartiainen, G. Masson, C. Breyer, D. Moser and E. Román Medina, *Progress in Photovoltaics: Research and Applications*, 2020, **28**, 439–453.

5 W. Cole and A. W. Frazier, *Cost Projections for Utility-Scale Battery Storage*, National renewable energy laboratory technical report, 2019.

6 Agora Verkehrswende, Agora Energiewende and Frontier Economics, *The Future Cost of Electricity-Based Synthetic Fuels*, Agora verkehrswende agora energiewende frontier economics technical report, 2018.

7 I. Tsiropoulos, D. Tarvydas and A. Zucker, *Cost development of low carbon energy technologies*, Jrc, european commission technical report, 2018.

8 IEA, *IEA G20 Hydrogen report: Assumptions*, International energy agency technical report, 2019.

9 International Energy Agency (IEA), *Capital cost of utility-scale battery storage systems in the New Policies Scenario, 2017-2040*, 2019, `https://www.iea.org/data-and-statistics/charts/capital-cost-of-utility-scale-battery-storage-systems-in-the-new-policies-scenario-2017-2040`.

10 Batstorm, *Battery storage to drive the power system transition*, Batstorm technical report, 2018.

11 P. Runge, C. Sölch, J. Albert, P. Wasserscheid, G. Zöttl and V. Grimm, *Economic comparison of electric fuels produced at excellent locations for renewable energies: A Scenario for 2035*, Fau technical report, 2020.

12 G. Matute, J. M. Yusta and L. C. Correas, *International Journal of Hydrogen Energy*, 2019, **44**, 17431–17442.

13 H. Böhm, A. Zauner, D. C. Rosenfeld and R. Tichler, *Applied Energy*, 2020, **264**, 114780.

14 J. Gorre, F. Ortloff and C. van Leeuwen, *Applied Energy*, 2019, **253**, 113594.

15 J. Michalski, U. Bünger, F. Crotogino, S. Donadei, G. S. Schneider, T. Pregger, K. K. Cao and D. Heide, *International Journal of Hydrogen Energy*, 2017, **42**, 13427–13443.

16 S. Brynolf, M. Taljegard, M. Grahn and J. Hansson, *Renewable and Sustainable Energy Reviews*, 2018, **81**, 1887–1905.

17 A. Buttler and H. Spliethoff, *Renewable and Sustainable Energy Reviews*, 2018, **82**, 2440–2454.

18 M. Fasihi, O. Efimova and C. Breyer, *Journal of Cleaner Production*, 2019, **224**, 957–980.

19 C. Beuttler, L. Charles and J. Wurzbacher, *Frontiers in Climate*, 2019, **1**, 10.

20 International Energy Agency, *Direct Air Capture: A key technology for net zero*, OECD, 2022.

21 Global Alliance Powerfuels, *Powerfuels Application Fields Factsheets about powerfuels technologies and their areas of application*, 2019.

22 N. McQueen, K. V. Gomes, C. McCormick, K. Blumanthal, M. Pisciotta and J. Wilcox, *Progress in Energy*, 2021, **3**, 032001.

23 J. Young, N. McQueen, C. Charalambous, S. Foteinis, O. Hawrot, M. Ojeda, H. Pilorgé, J. Andresen, P. Psarras, P. Renforth, S. Garcia and M. v. d. Spek, *One Earth*, 2023, **6**, 899–917.

24 S. Shayegh, V. Bosetti and M. Tavoni, *Frontiers in Climate*, 2021, **3**, year.

25 S. Fuss, W. F. Lamb, M. W. Callaghan, J. Hilaire, F. Creutzig, T. Amann, T. Beringer, W. de Oliveira Garcia, J. Hartmann, T. Khanna, G. Luderer, G. F. Nemet, J. Rogelj, P. Smith, J. L. V. Vicente, J. Wilcox, M. del Mar Zamora Dominguez and J. C. Minx, *Environmental Research Letters*, 2018, **13**, 063002.

26 K. Lebling, H. Leslie-Bole, Z. Byrum and L. Bridgwater, 2022.

27 BCG, *Shifting the Direct Air Capture Paradigm*, 2023.

28 K. S. Lackner and H. Azarabadi, *Industrial & Engineering Chemistry Research*, 2021, **60**, 8196–8208.

29 S. Haas, B. Schachler and U. Krien, *windpowerlib - a python library to model wind power plants*, 2019, `https://zenodo.org/record/3403360`.

30 B. Graver, *U.S. Airlines On Track To Meet One Carbon Goal, Even Without Government Leadership*, International council on clean transportation technical report, 2018.